Mass Determination in SUSY-like Events with Missing Energy

Jack Gunion
U.C. Davis

Collaborators: Hsin-Chia Cheng, Zhenyu Han, Guido Marandella, Bob McElrath

CERN, July 2007

Fundamental physics goals for the LHC and the ILC

1. **Discover and understand in detail the mechanism for EWSB.**

   Higgs bosons, e.g.

2. **Determine if the hierarchy problem has been solved or not.**

   SUSY?

3. **Discover the dark matter particle(s) and measure the properties of all particles needed for computing the relic density.**

   R-parity conserving SUSY for example.

4. **Explain electroweak or other baryogenesis using particles seen at the LHC and ILC.**

Attractive models simultaneously solve at least the **hierarchy and dark matter** problems simultaneously through the introduction of new particles with masses below the TeV scale, the lightest of which is absolutely stable and therefore a good dark matter candidate.

Given the probable ILC time scales, the big question is if the LHC alone will be able to verify that any new particles discovered really do the job.

A very crucial part of the answer involves the accuracy with which mass scales can be determined at the LHC in the presence of missing energy!

Missing Energy: Motivations, Models and Implications

There are two very important reasons to suppose that LHC events will contain missing energy due to a pair of neutral stable weakly-interacting particles.

1. **The correct amount of dark matter relic density is easily achieved if there is a neutral stable TeV scale WIMP — this is almost an independent argument for new physics at the TeV scale.**

   Such a WIMP must be very weakly interacting (if = dark matter) and will therefor 'appear' as missing energy in the LHC detectors.

2. **A new parity associated with the WIMP's (assuming they are at the $\lesssim$ TeV scale) is strongly suggested by precision electroweak data.**

   Precision electroweak observables would be very significantly impacted if there are vertices connecting a single particle of the WIMP family to SM particles.

   If there is a discrete symmetry that only allows a pair of new particles to connect to a SM-particle $\Rightarrow$ all effects at the loop-level.

Then, automatically the lightest particle in this new family will be stable and will escape detection if it is neutral and weakly interacting.

Popular Candidate Models

- **SUSY with R-parity conservation.**

  The lightest supersymmetric particle (LSP) is likely to be a neutralino, which is a good WIMP candidate.

- **Little Higgs Models with T-parity: lightest T-odd particle is a good WIMP.**

- **Universal Extra Dimensions: lightest KK mode (e.g. first excited 'photon') is a good WIMP.**

- **Models with warped unification with Z_3 parity, ...**

All produce events of similar topologies.

The problem: In general, if there is a pair of invisible particles, then there is not enough information to reconstruct the kinematics of each event *on an event-by-event basis*.

- **Mass scales will be important not only for the dark matter issue but also for the LHC inverse problem: Can we use LHC data to determine the fundamental Lagrangian parameters?**
  And, can we do so with sufficient accuracy as to allow a meaningful extrapolation to the GUT scale?
  The general picture:

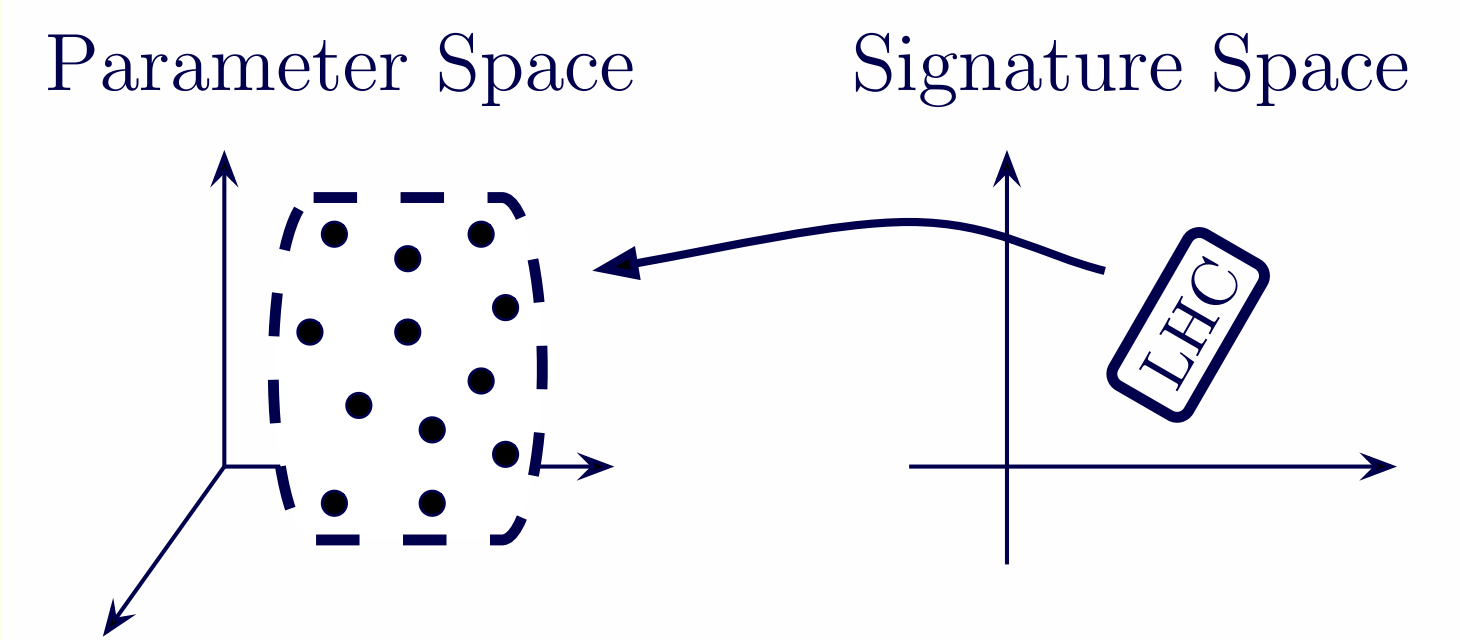

Figure 1: *The likely LHC situation.* *N. Arkani-Hamed, G. L. Kane, J. Thaler and L. T. Wang, JHEP* **0608**, *070 (2006) [arXiv:hep-ph/0512190].*

The picture is particularly bad if the LHC will have a hard time determining the absolute mass scale.

As an example of the difficulties encountered, let us consider the mSUGRA SPS1a' point. It gives a spectrum of the following type:

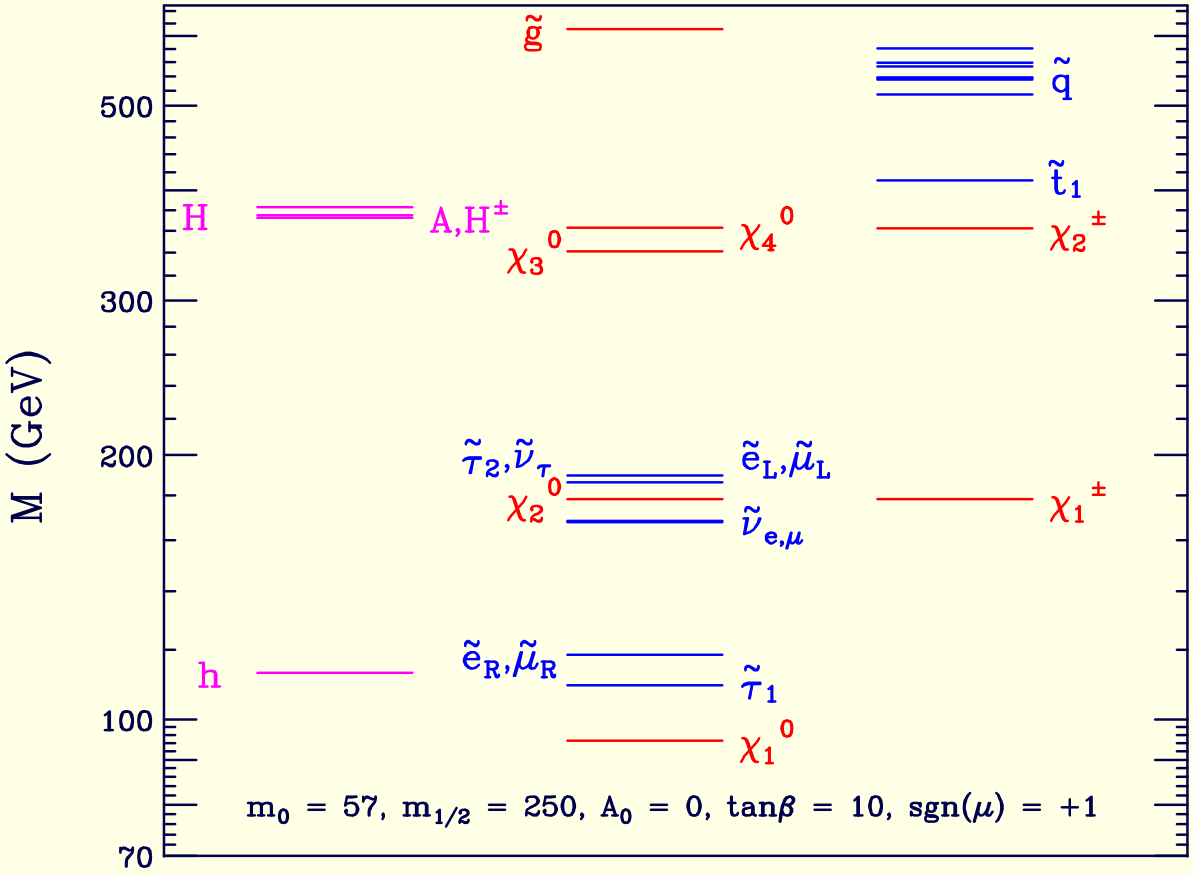

Figure 2: *Mass spectra of an SPS1a'-like point.*

Using lepton spectrum edges and the like, one gets quite a bit of information about the spectrum, but a good determination of the overall mass scale is

elusive. $m_{\widetilde{\chi}_1^0}$ sets the overall scale.

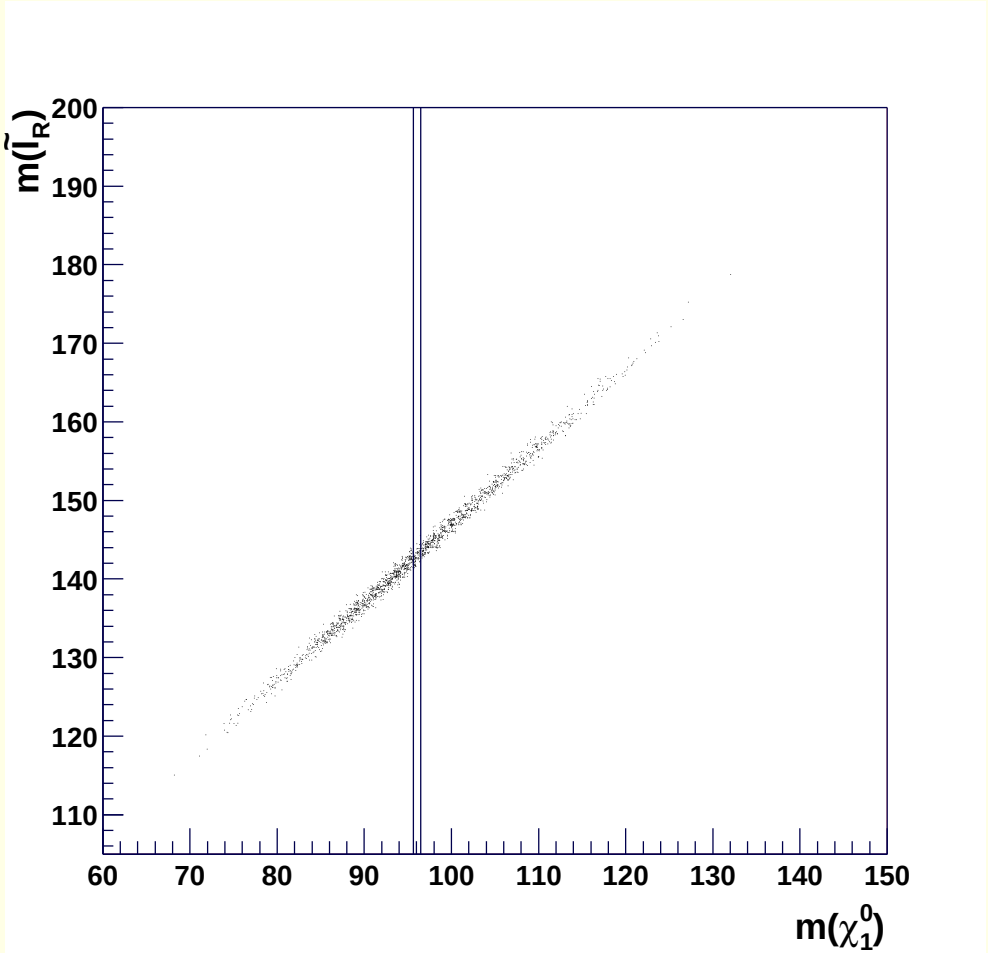

Figure 3: *Sample mass correlation plot. Dots: LHC alone; Vertical band* $= \pm 2\sigma$ *for ILC data. G. Weiglein et al. [LHC/LC Study Group], Phys. Rept.* **426**, *47 (2006) [arXiv:hep-ph/0410364]. Note: These results are for the SPS1a' 'dot'.*

How does such LHC accuracy compare to what is needed?

a) A precision calculation of the dark matter primarily needs accurate masses (couplings being fixed by supersymmetry). The ILC measures $m_{\widetilde{\chi}_1^0}$ and other masses to within $\Delta m_{\widetilde{\chi}_1^0} \sim \pm 3$ GeV. Could we possibly reach this level at the LHC?

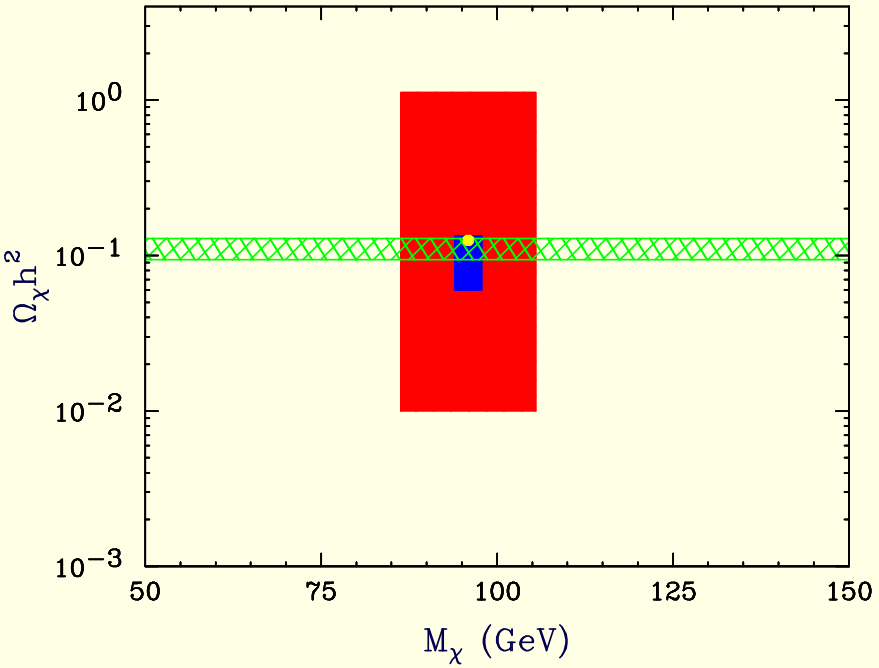

Figure 4: *Accuracy of WMAP (horizontal green shaded region), LHC (outer red rectangle) and ILC (inner blue rectangle) in determining $m_{\widetilde{\chi}_1^0}$, the mass of the lightest neutralino, and its relic density $\Omega_\chi h^2$. LHC is assumed to get 10% accuracy on absolute $m_{\widetilde{\chi}_1^0}, m_{\widetilde{\chi}_2^0}, m_{\widetilde{\chi}_1^\pm}$ masses = optimistic using usual techniques. The yellow dot denotes the actual values of $m_{\widetilde{\chi}_1^0}$ and $\Omega_\chi h^2$ for point B'. A. Birkedal, et al.hep-ph/0507214*

b) Precision mass measurement are needed to meaningfully assess GUT scale boundary conditions.

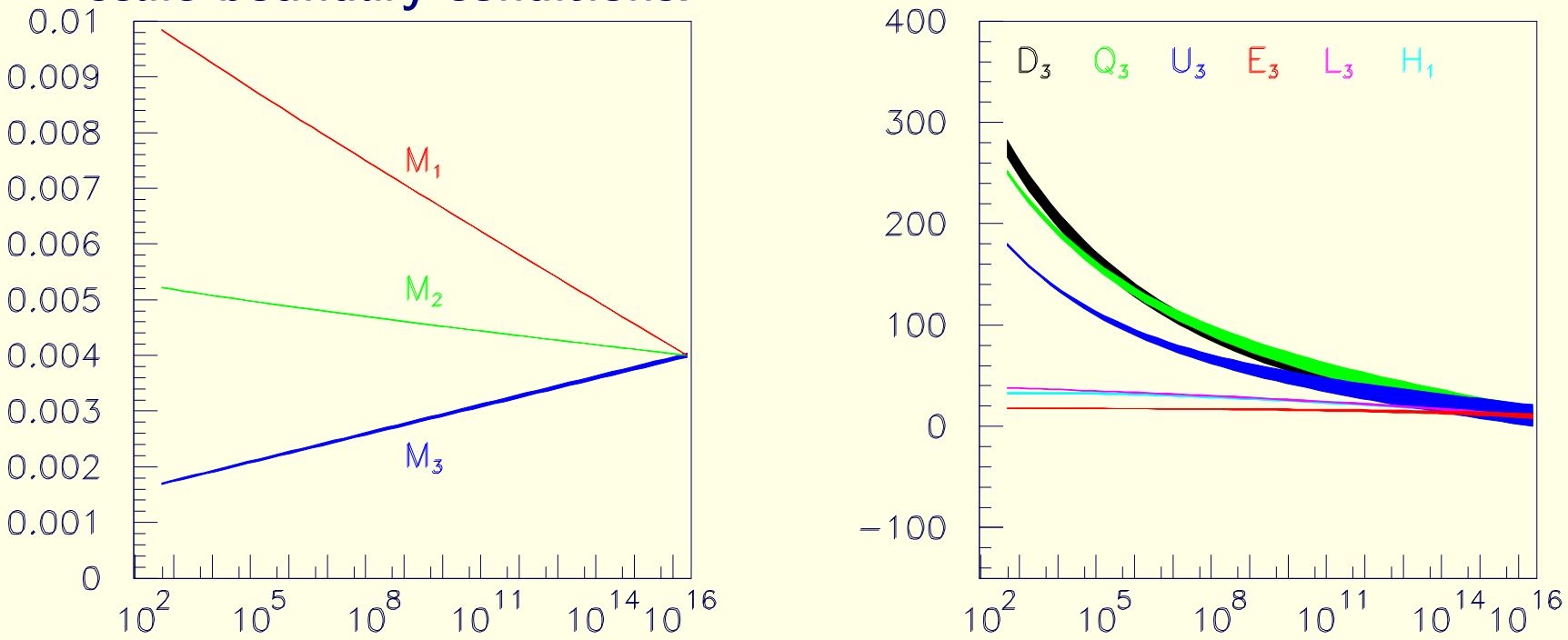

Figure 5: *Evolution to the GUT scale using LHC + ILC1000 measurements. On the left,* $1/M_i$ *[GeV*$^{-1}$*] is plotted vs.* Q(GeV). *On the right,* $M^2_{\tilde{j}}$ *[*10^3 *GeV*^{2}*] for 3rd soft masses squared are plotted vs.* Q(GeV).

Differences between sparticle masses are determined at the LHC, but, will it require the ILC (e.g. via threshold scans) to get the absolute mass scales.

We must work to get absolute masses with the required accuracy using LHC data alone.

Basic Constraint Counting

One chain examples

1. The "marginal" case is 3 visible particles (or combinations of particles) with 3 on-shell resonances involved and 1 final invisible particle:

$$Z \to Y v_1 \to X v_2 v_1 \to N v_3 v_2 v_1 \tag{1}$$

   For this case, after n events, the number of unknowns is 4 masses and $4n$ 4-momenta of the final invisible particle (N).

   The number of on-shell constraints from requiring given Z, Y, X, N masses in each event is $4n$.

   Thus, the number of unknowns is always $4 + 4n - 4n = 4$ (the masses) no matter how many events.

2. For 4 visible particles with 4 on-shell resonances and the final N, after n events there are $5 + 4n$ unknowns and $5n$ constraints, implying equality

when $n = 5$. So, if there were no combinatoric / resolution issues, $n = 5$ events would allow you to solve for the 5 masses aside from discrete quartic equation solution ambiguities.

Two chain examples

1. The "marginal" case here is just two visible particles per chain: $Y \to Xv_1 \to Nv_2v_1$.

   If we assume equal masses on the two chains, then there are 3 unknown masses, including m_N.

   For each event, there are the two 4-momenta of the two final N's, but we know the sum of their transverse momenta from balancing against the visible particle transverse momenta, implying 6 unknown momenta components per event.

   After n events, the number of unknowns is then $3 + 6n$.

   The number of constraints is $6n$ (since we assume on-shell masses on both chains.)

   Thus, no matter how many events, we always have the 3 unknown mass parameters that cannot be absolutely solved for.

Note that by considering both chains, we are at the marginal situation with just 2 visible particles and 2 on-shell resonances plus the 1 final invisible particle, as opposed to the one-chain case where marginality required 3 visible particles, corresponding to 3 on-shell resonances plus 1 invisible particle.

2. The first non-marginal case is clearly 3 visible particles *per chain*, corresponding to $3 + 1 = 4$ unknown masses.

   In this case, after n events we have $4 + 6n$ unknowns and $8n$ on-shell constraints (recall we have two chains each of which has four mass constraints) implying solution (subject to discrete ambiguities) when $4 + 6n - 8n = 0 \Rightarrow n = 2$.

   Again, there is a reduction in the number of on-shell resonances and associated visible particles that are needed to get discrete solutions, as compared to considering a single chain.

A significant problem with both the 1-chain and 2-chain approaches is combinatorics.

For example, for the decay chain $\widetilde{q} \to q\widetilde{\chi}_2^0 \to q\mu\widetilde{\mu}_R \to q\mu\mu\widetilde{\chi}_1^0$ in $\widetilde{q}\widetilde{q}$ production, in each event there would be $2!$ ways to place the q's and

$4 \times 2 \times 2$ ways to place the μ's (noting that each chain has to have one μ^+ and one μ^-, but we don't know which comes first.) The net is $2 \times 16 = 32$ ways of placing particles.

If there are additional jets from ISR and / or from $\widetilde{g}\widetilde{q}$ and $\widetilde{g}\widetilde{g}$ production, there would be additional combinatoric possibilities or else one would need to implement a selection criterion for choosing the jets that one hoped came from $\widetilde{q}$ decays directly.

Previous LHC Work

- Observables such as H_T, $M_{\rm eff}$ . . . $\Rightarrow$ are sensitive to the mass differences of the particles in the decay chains as revealed by visible particles in the chain decays, but cancellation of $\not{p}_T$ between chains means they are not very sensitive to the overall mass scale.

- If the model is known and all branching ratios for the different chain decay sequences can be computed, then total cross sections and distribution shapes for different topologies can be used to determine the absolute scale.

  But, this is really very model-dependent.

- One would like to use pure kinematics to get the absolute masses.

  How well one can do and the best techniques depends very much on the topology of the events.

- For a long enough chain decay, one can use multiple endpoints. But, as per the example above, this gets mass differences but not absolute masses.

And, it certainly doesn't work if there are only two visible particles — only one invariant mass that can be formed $\Rightarrow$ too few constraints.

- **For example, for the 3-step topology below, one looks for endpoints in $m_{\ell\ell}$, $m_{q\ell\ell}$, $m_{q\ell}^{high}$, and $m_{q\ell}^{low}$.**

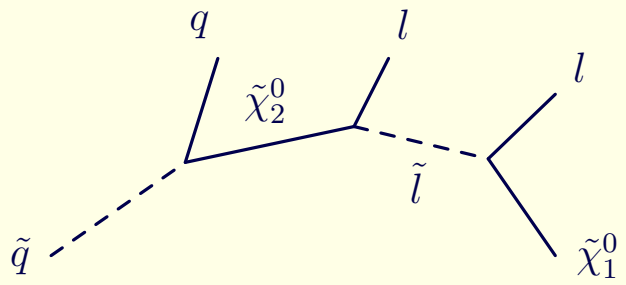

Figure 6: *The SPS1a' type squark decay chain.* $\widetilde{q} \longrightarrow q\ell\ell\widetilde{\chi}_1^0$.

$$\left(m_{ll}^{\max}\right)^2 = \left(m_{\tilde{\chi}_2^0}^2 - m_{\tilde{l}_R}^2\right)\left(m_{\tilde{l}_R}^2 - m_{\tilde{\chi}_1^0}^2\right)/m_{\tilde{l}_R}^2$$

$$\left(m_{qll}^{\max}\right)^2 = \begin{cases} \dfrac{\left(m_{\tilde{q}_L}^2 - m_{\tilde{\chi}_2^0}^2\right)\left(m_{\tilde{\chi}_2^0}^2 - m_{\tilde{\chi}_1^0}^2\right)}{m_{\tilde{\chi}_2^0}^2} & \text{for} \quad \dfrac{m_{\tilde{q}_L}}{m_{\tilde{\chi}_2^0}} > \dfrac{m_{\tilde{\chi}_2^0}}{m_{\tilde{l}_R}}\dfrac{m_{\tilde{l}_R}}{m_{\tilde{\chi}_1^0}} \quad (1) \\ \dfrac{\left(m_{\tilde{q}_L}^2 m_{\tilde{l}_R}^2 - m_{\tilde{\chi}_2^0}^2 m_{\tilde{\chi}_1^0}^2\right)\left(m_{\tilde{\chi}_2^0}^2 - m_{\tilde{l}_R}^2\right)}{m_{\tilde{\chi}_2^0}^2 m_{\tilde{l}_R}^2} & \text{for} \quad \dfrac{m_{\tilde{\chi}_2^0}}{m_{\tilde{l}_R}} > \dfrac{m_{\tilde{l}_R}}{m_{\tilde{\chi}_1^0}}\dfrac{m_{\tilde{q}_L}}{m_{\tilde{\chi}_2^0}} \quad (2) \\ \dfrac{\left(m_{\tilde{q}_L}^2 - m_{\tilde{l}_R}^2\right)\left(m_{\tilde{l}_R}^2 - m_{\tilde{\chi}_1^0}^2\right)}{m_{\tilde{l}_R}^2} & \text{for} \quad \dfrac{m_{\tilde{l}_R}}{m_{\tilde{\chi}_1^0}} > \dfrac{m_{\tilde{q}_L}}{m_{\tilde{\chi}_2^0}}\dfrac{m_{\tilde{\chi}_2^0}}{m_{\tilde{l}_R}} \quad (3) \\ \left(m_{\tilde{q}_L} - m_{\tilde{\chi}_1^0}\right)^2 & \text{otherwise} \quad (4) \end{cases}$$

$$\left(m_{ql(\mathrm{low})}^{\max}, m_{ql(\mathrm{high})}^{\max}\right) = \left\{ \begin{array}{lll} \left(m_{ql_{\mathrm{n}}}^{\max}, m_{ql_{\mathrm{f}}}^{\max}\right) & \text{for} & 2m_{\tilde{l}_R}^2 > m_{\tilde{\chi}_1^0}^2 + m_{\tilde{\chi}_2^0}^2 > 2m_{\tilde{\chi}_1^0} m_{\tilde{\chi}_2^0} \quad (1) \\ \left(m_{ql(\mathrm{eq})}^{\max}, m_{ql_{\mathrm{f}}}^{\max}\right) & \text{for} & m_{\tilde{\chi}_1^0}^2 + m_{\tilde{\chi}_2^0}^2 > 2m_{\tilde{l}_R}^2 > 2m_{\tilde{\chi}_1^0} m_{\tilde{\chi}_2^0} \quad (2) \\ \left(m_{ql(\mathrm{eq})}^{\max}, m_{ql_{\mathrm{n}}}^{\max}\right) & \text{for} & m_{\tilde{\chi}_1^0}^2 + m_{\tilde{\chi}_2^0}^2 > 2m_{\tilde{\chi}_1^0} m_{\tilde{\chi}_2^0} > 2m_{\tilde{l}_R}^2 \quad (3) \end{array} \right\}$$

$$\left(m_{ql_{\mathrm{n}}}^{\max}\right)^2 = \left(m_{\tilde{q}_L}^2 - m_{\tilde{\chi}_2^0}^2\right)\left(m_{\tilde{\chi}_2^0}^2 - m_{\tilde{l}_R}^2\right)/m_{\tilde{\chi}_2^0}^2$$

$$\left(m_{ql_{\mathrm{f}}}^{\max}\right)^2 = \left(m_{\tilde{q}_L}^2 - m_{\tilde{\chi}_2^0}^2\right)\left(m_{\tilde{l}_R}^2 - m_{\tilde{\chi}_1^0}^2\right)/m_{\tilde{l}_R}^2$$

$$\left(m_{ql(\mathrm{eq})}^{\max}\right)^2 = \left(m_{\tilde{q}_L}^2 - m_{\tilde{\chi}_2^0}^2\right)\left(m_{\tilde{l}_R}^2 - m_{\tilde{\chi}_1^0}^2\right)/\left(2m_{\tilde{l}_R}^2 - m_{\tilde{\chi}_1^0}^2\right)$$

$$\begin{aligned} \left(m_{qll(\theta>\frac{\pi}{2})}^{\min}\right)^2 = & \left[\left(m_{\tilde{q}_L}^2 + m_{\tilde{\chi}_2^0}^2\right)\left(m_{\tilde{\chi}_2^0}^2 - m_{\tilde{l}_R}^2\right)\left(m_{\tilde{l}_R}^2 - m_{\tilde{\chi}_1^0}^2\right)\right. \\ & -\left(m_{\tilde{q}_L}^2 - m_{\tilde{\chi}_2^0}^2\right)\sqrt{\left(m_{\tilde{\chi}_2^0}^2 + m_{\tilde{l}_R}^2\right)^2\left(m_{\tilde{l}_R}^2 + m_{\tilde{\chi}_1^0}^2\right)^2 - 16m_{\tilde{\chi}_2^0}^2 m_{\tilde{l}_R}^4 m_{\tilde{\chi}_1^0}^2} \\ & \left.+2m_{\tilde{l}_R}^2\left(m_{\tilde{q}_L}^2 - m_{\tilde{\chi}_2^0}^2\right)\left(m_{\tilde{\chi}_2^0}^2 - m_{\tilde{\chi}_1^0}^2\right)\right]/\left(4m_{\tilde{l}_R}^2 m_{\tilde{\chi}_2^0}^2\right) \end{aligned}$$

- **However, to get the absolute mass scale you need to use distribution shapes as well as endpoints as in Gjeltsen, Miller, Osland: hep-ph/0410303.**

  This, however, is rather model dependent, and even doing so still leaves discrete ambiguities for the absolute scale.

  The cases they analyzed were a low-mass SPS1a-like scenario and a high-mass scenario along the SPS1a line with lower event rate.

Point	$\tilde{g}$	$\tilde{d}_L$	$\tilde{d}_R$	$\tilde{u}_L$	$\tilde{u}_R$	$\tilde{b}_2$	$\tilde{b}_1$	$\tilde{t}_2$	$\tilde{t}_1$
(α)	595.2	543.0	520.1	537.2	520.5	524.6	491.9	574.6	379.1
(β)	915.5	830.1	799.5	826.3	797.3	800.2	759.4	823.8	610.4
	$\tilde{e}_L$	$\tilde{e}_R$	$\tilde{\tau}_2$	$\tilde{\tau}_1$	$\tilde{\nu}_{e_L}$	$\tilde{\nu}_{\tau_L}$		$H^{\pm}$	A
(α)	202.1	143.0	206.0	133.4	185.1	185.1		401.8	393.6
(β)	315.6	221.9	317.3	213.4	304.1	304.1		613.9	608.3
	$\tilde{\chi}_4^0$	$\tilde{\chi}_3^0$	$\tilde{\chi}_2^0$	$\tilde{\chi}_1^0$	$\tilde{\chi}_2^{\pm}$	$\tilde{\chi}_1^{\pm}$		H	h
(α)	377.8	358.8	176.8	96.1	378.2	176.4		394.2	114.0
(β)	553.3	538.4	299.1	161.0	553.3	299.0		608.9	117.9

Table 1: *Masses [GeV] for the considered SPS 1a points (α: $m_0 = 100$ GeV, $m_{1/2} = 250$ GeV) and (β: $m_0 = 160$ GeV, $m_{1/2} = 400$ GeV).*

For $L = 300$ fb^{-1}

	Nom	(1,1) $\langle m \rangle$	(1,1) σ	(1,1) γ_1	(1,2) $\langle m \rangle$	(1,2) σ	(1,2) γ_1
$m_{\tilde{\chi}_1^0}$	96.1	96.3	3.8	0.2	85.3	3.4	0.1
$m_{\tilde{l}_R}$	143.0	143.2	3.8	0.2	130.4	3.7	0.1
$m_{\tilde{\chi}_2^0}$	176.8	177.0	3.7	0.2	165.5	3.4	0.1
$m_{\tilde{q}_L}$	537.2	537.5	6.1	0.1	523.2	5.1	0.1
$m_{\tilde{b}_1}$	491.9	492.4	13.4	0.0	469.6	13.3	0.1
$m_{\tilde{l}_R} - m_{\tilde{\chi}_1^0}$	46.92	46.93	0.28	0.0	45.08	0.72	−0.2
$m_{\tilde{\chi}_2^0} - m_{\tilde{\chi}_1^0}$	80.77	80.77	0.18	0.0	80.18	0.29	−0.1
$m_{\tilde{q}_L} - m_{\tilde{\chi}_1^0}$	441.2	441.3	3.1	0.0	438.0	2.7	0.0
$m_{\tilde{b}_1} - m_{\tilde{\chi}_1^0}$	395.9	396.2	12.0	0.0	384.4	12.0	0.1

Table 2: *SPS 1a (α): Minima for $\Delta\Sigma \leq 1$ in regions (1,1) and (1,2). Ensemble means, $\langle m \rangle$, and root-mean-square distances from the mean, σ, are in GeV. The three lightest masses are very correlated. The mass of $\tilde{q}_L$ is fairly correlated to the lighter masses, but $m_{\tilde{b}_1}$ is essentially uncorrelated. The distributions are very close to symmetric.* **Note the wrong solution region.**

- **It gets worse as masses increase (and therefore event rates decrease).**

For $L = 300$ fb^{-1}

		1 solution						2 solutions					
		(1,1)			*(1,2)/(1,3)*/B			*(1,2)*			*(1,3)*		
	Nom	$\langle m \rangle$	σ	γ_1	$\langle m \rangle$	σ	γ_1	$\langle m \rangle$	σ	γ_1	$\langle m \rangle$	σ	γ_1
$\tilde{\chi}_1^0$	161	438	88	0.9	175	35	1.0	161	22	0.3	166	27	0.6
$\tilde{l}_R$	222	518	85	0.7	236	37	0.8	221	24	0.3	223	28	0.5
$\tilde{\chi}_2^0$	299	579	85	0.7	313	35	1.0	299	22	0.3	304	27	0.6
$\tilde{q}_L$	826	1146	104	0.8	843	44	0.9	826	30	0.3	835	36	0.5
$\tilde{l}_R - \tilde{\chi}_1^0$	61	81	1.8	−0.3	61	4.4	0.4	61	1.9	−0.2	57	1.3	−0.2
$\tilde{\chi}_2^0 - \tilde{\chi}_1^0$	138	141	0.9	0.1	138	0.6	0.2	138	0.5	0.0	138	0.5	0.0
$\tilde{q}_L - \tilde{\chi}_1^0$	665	708	17	0.1	668	10	0.5	665	9	0.1	669	10	0.2

Table 3: *SPS 1a (β): Nominal masses ('Nom') and $\Delta\Sigma \leq 1$ ensemble distribution values for the three solution types. High-mass sector: The (1,1) solutions return masses far beyond the nominal values. Low-mass sector: For the one-solution case the values are based on the common distribution of (1,2), (1,3) and border (B) solutions. In the two-solution case the ensemble variables of both solutions are shown. Ensemble means, $\langle m \rangle$, and root-mean-square values, σ, are in GeV.* **Note how some absolute mass scale solutions are way off.**

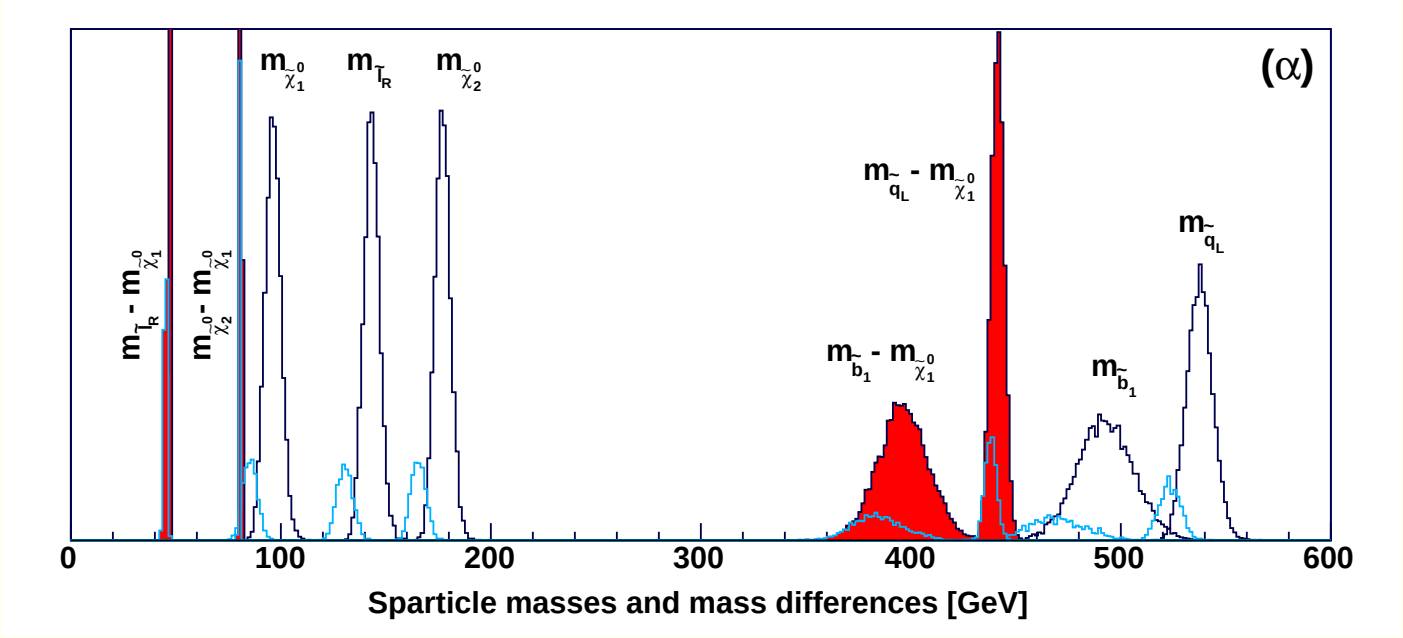

Figure 7: *Plots of mass differences and absolute masses for The SPS1a' type squark decay chain* α.

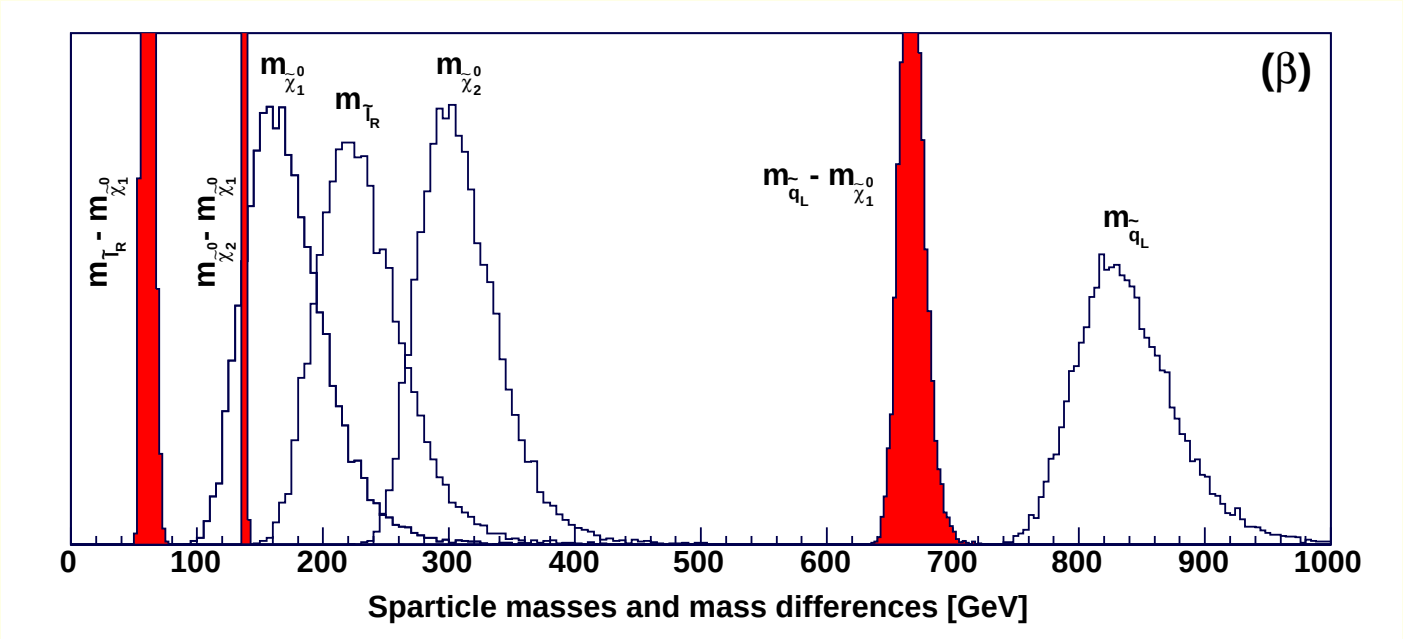

Figure 8: *Plots of mass differences and absolute masses for The SPS1a' type squark decay chain* β.

- **Another analysis of exactly the same decay chain: A.J. Barr, C.G. Lester, M.A. Parker: hep-ph/050843**

  They use only the edges, not the distribution shapes of the invariant mass distributions.

  They choose a point consistent with the WMAP data, described by the following set of mSUGRA parameters:

$$m_0 = 70 \text{ GeV},\ m_{1/2} = 350 \text{ GeV},\ \tan\beta = 10,\ A_0 = 0,\ \mu > 0$$

yielding

Particle	Mass (GeV)
$\tilde{\chi}_1^0$	137
$\tilde{\chi}_2^0$	264
$\tilde{e}_L$	255
$\tilde{e}_R$	154
$\tilde{g}$	832
$\tilde{u}_L$	760
$\tilde{u}_R$	735
$\tilde{d}_L$	764
$\tilde{d}_R$	733

Particle	Mass (GeV)
$\tilde{b}_1$	698
$\tilde{b}_2$	723
$\tilde{t}_1$	574
$\tilde{t}_2$	749
$\tilde{\tau}_1$	147
$\tilde{\tau}_2$	257
h	116

Table 4: *The most important sparticle masses at the coannihilation point.*

$L = 100$ fb^{-1}

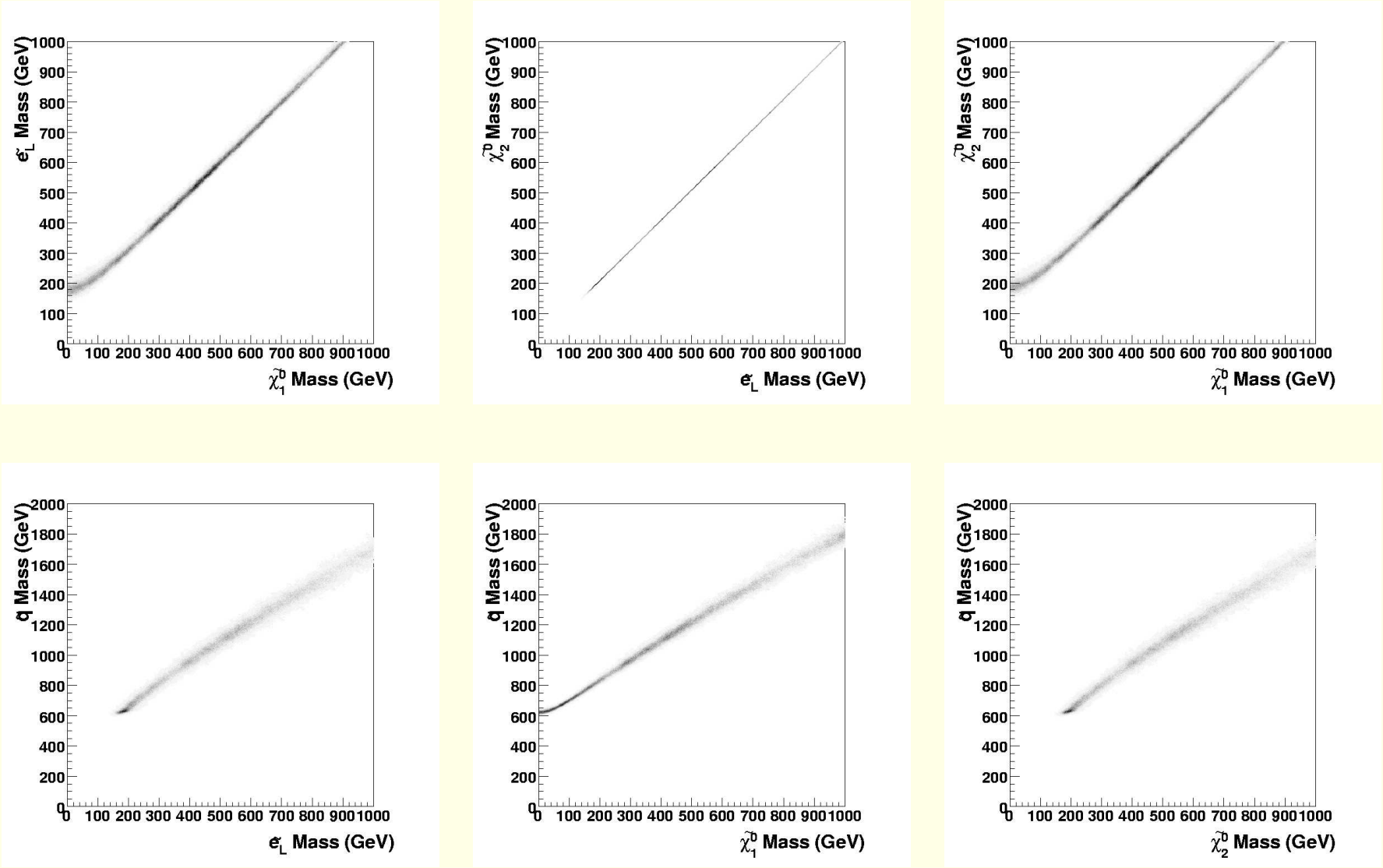

Figure 9: *The region of mass space consistent with the kinematic edge measurements described in the text, obtained using a Markov chain sampler.*

$L = 100$ fb^{-1}

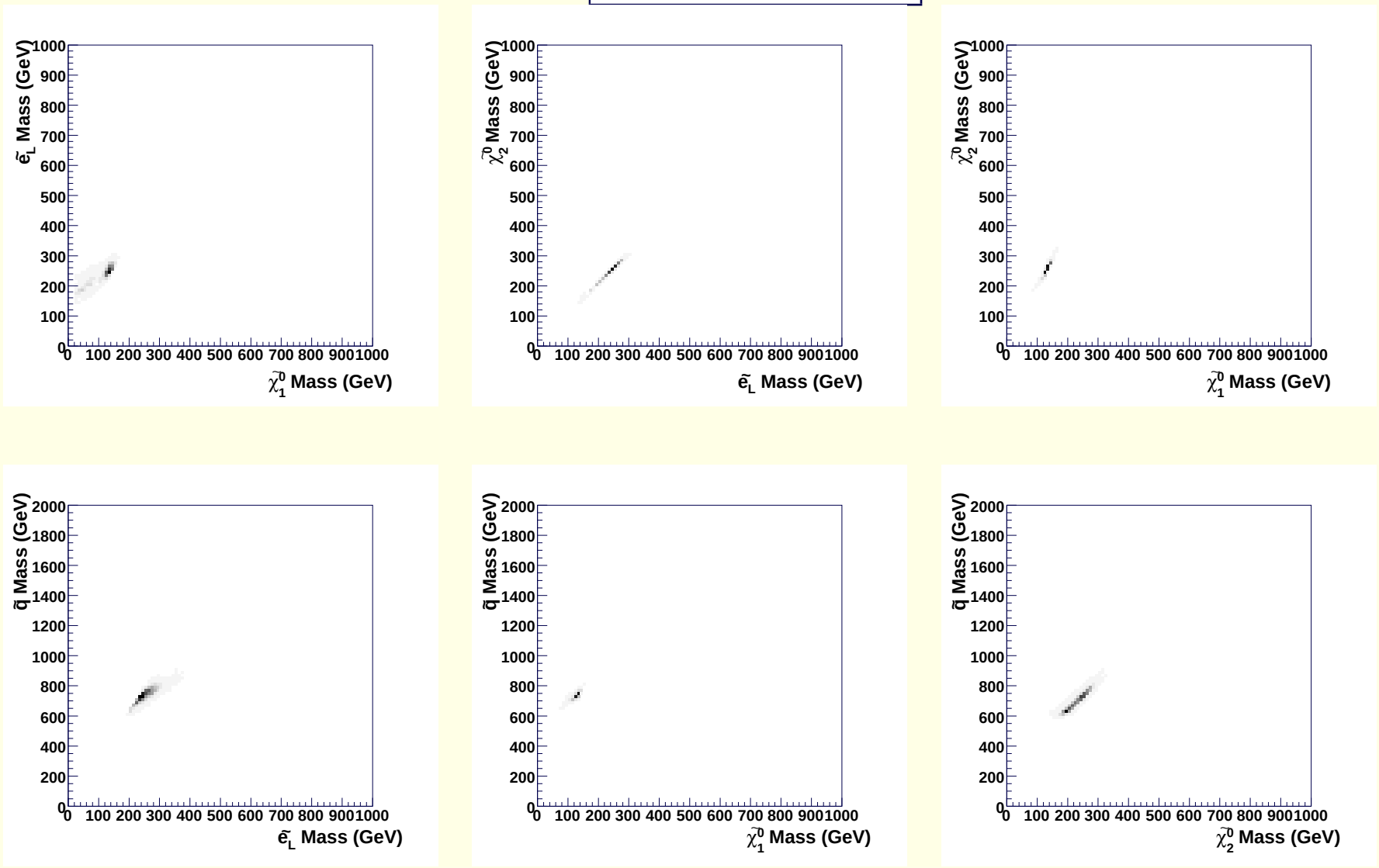

Figure 10: *The region of mass space consistent with a measurement at 10% precision of the cross-section of events with missing p_T greater than 500 GeV, overlapped with a measurement of the squark decay kinematic endpoints. Cross section inputs $\Rightarrow$ much better, but model-dependent and still not wonderful.*

- **The one-chain non-marginal case was considered in Kawagoe, Nojiri, Polesello, hep-ph/0312317, hep-ph/0410160.**

  They employed the SUSY example:

$$\widetilde{g} \to \widetilde{b} b_2 \to \widetilde{\chi}_2^0 b_1 b_2 \to \widetilde{l} b_1 b_2 \ell_1 \to \widetilde{\chi}_1^0 b_1 b_2 \ell_1 \ell_2 \tag{9}$$

  The constraint equations are:

$$\begin{aligned} m^2_{\widetilde{\chi}_1^0} &= p^2_{\widetilde{\chi}_1^0} \\ m^2_{\widetilde{\ell}} &= (p_{\widetilde{\chi}_1^0} + p_{\ell_1})^2 \\ m^2_{\widetilde{\chi}_2^0} &= (p_{\widetilde{\chi}_1^0} + p_{\ell_1} + p_{\ell_2})^2 \\ m^2_{\widetilde{b}} &= (p_{\widetilde{\chi}_1^0} + p_{\ell_1} + p_{\ell_2} + p_{b_1})^2 \\ m^2_{\widetilde{g}} &= (p_{\widetilde{\chi}_1^0} + p_{\ell_1} + p_{\ell_2} + p_{b_1} + p_{b_2})^2 \end{aligned} \tag{10}$$

  Recall from the counting that for each set of 5 events we should get a unique solution in principle, and all should agree. (mod discrete ambiguities)

  In practice, this is not what they did.

Before going on, the important point of the long chain decay should now be clear.

Even though there are two neutralinos produced in each collider event, *if we can isolate the* **3** *visible particles in the decay of a given gluino* then we don't care about what the other gluino is doing. It will just add to our statistics.

Well, there are combinatorics/misassignment issues here of course.

Anyway, what they actually did in their papers is as follows.

They assume that $m_{\tilde{\chi}_1^0}$, $m_{\tilde{\chi}_2^0}$ and $m_{\tilde{\ell}}$ are measured from endpoints (maybe also ILC) with great precision (as we have seen, if we only have LHC data this is not so perfect an assumption).

In this case, the unknown masses are $m_{\tilde{g}}$ and $m_{\tilde{b}}$.

For n events we have $2 + 4n$ unknowns and $5n$ constraints (keeping in mind that we assume or know masses for all five particles). $2 + 4n = 5n$ implies that in a perfect world we only need $n = 2$ events to get a unique solution.

In reality, must include combinatorics, resolution and backgrounds and the final result is phrased in terms of likelihood contours. In their words:

"The likelihood distribution peaks at the gluino and sbottom mass difference as 99.5 GeV for $\tan\beta = 10$, 104.2 GeV for $\tan\beta = 15$, and 113.9 GeV for $\tan\beta = 20$, where the input value is 103.3 GeV, 109.9 GeV and 116.5 GeV, respectively. The fitted values display shift of about 4 GeV from the true value. We ascribe this effect to our simplified modeling of the jet smearing in building the likelihood function, which should disappear once the detector response is properly taken into account in the unfolding procedure."

Well, there is a lot hidden in this phrase, but a very thorough understanding of the detector is clearly required.

- With this long-winded warm-up, I now turn to our procedure which we claim is: a) more robust; b) of greater general applicability; c) yields at the moment similar errors, but with further improvement likely.

2 chains — 2 visible particles per chain

- **We claim that one can do well at the LHC by taking a more global point of view and using as much information as is available in every event.**

  Our approach can be applied to many different types of event topologies, but here we focus on a subcomponent of the SPS1a type event in a way that has not been previously attempted.

  Consider the chain decay sequence:

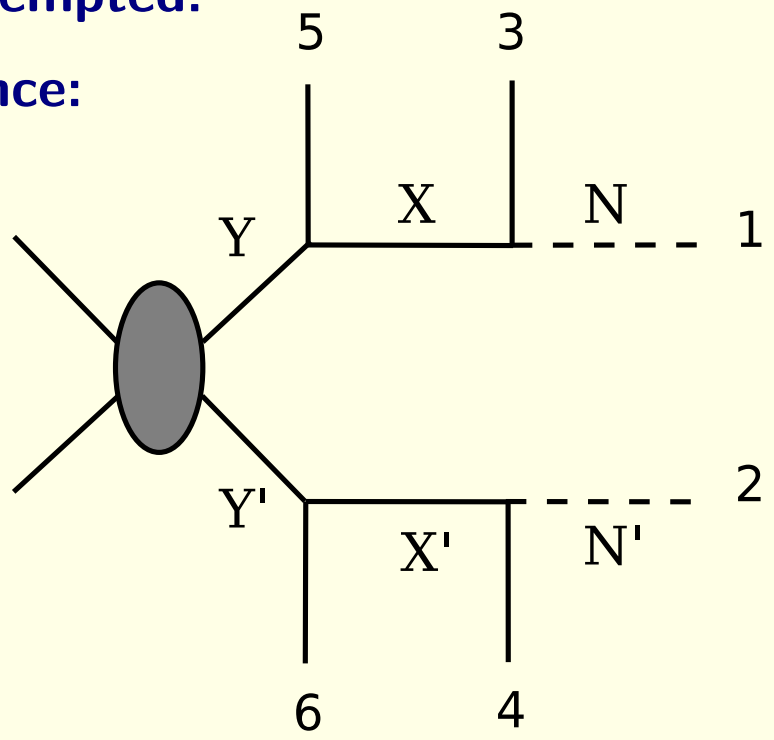

Figure 11: *A typical chain decay topology.*

Note: some cuts to isolate a given topology are required (just as in the previous analyzes) — perhaps OSET would do the job. By this, we don't mean perfect isolation — roughly a ratio of $S/B > 2$ is certain to work, where B could include old physics and new physics signals of other topologies. Even $S/B \sim 1$ is probably workable.

This topology can be applied to many processes with 4 visible and 2 invisible particles.

For example, suppose $M_Y = M_{Y'}$, $M_X = M_{X'}$, and $M_N = M_{N'}$.

Examples that fit this:

$$
\begin{aligned}
t\bar{t} &\rightarrow bW^+bW^- \rightarrow bl^+\nu bl^-\bar{\nu} \\
\tilde{\chi}_2^0\tilde{\chi}_2^0 &\rightarrow l\tilde{l}l\tilde{l} \rightarrow ll\tilde{\chi}_1^0ll\tilde{\chi}_1^0 \\
\tilde{q}\tilde{q} &\rightarrow q\tilde{\chi}_2^0q\tilde{\chi}_2^0 \rightarrow ql\tilde{l}ql\tilde{l} \rightarrow qll\tilde{\chi}_1^0qll\tilde{\chi}_1^0 \\
\tilde{t}\bar{\tilde{t}} &\rightarrow b\tilde{\chi}^+\bar{b}\tilde{\chi}^- \rightarrow bW^+\tilde{\chi}_1^0\bar{b}W^-\tilde{\chi}_1^0
\end{aligned}
$$

The third entry above is the SPS1a' case of interest.

Let us count the constraints and unknowns once again. For this we (temporarily) assume that the particles are exactly on-shell and that experimental resolutions are perfect.

1. There are 8 unknowns corresponding to the 4-momenta of the N and N'.

2. There are 2 constraints on these coming from knowledge of the visible transverse momenta. (We are assuming that the longitudinal momentum and energy of the collision is not known, as appropriate at a hadron collider.)

   If there are extra visible jets in the event we just include them in visible $\vec{p}_T$.

   The visible particles 3, 4, 5 and 6 need not be stable. We just need to be able to determine their 4-momenta (e.g. $W \to jj$ is ok but $W \to \ell\nu$ is not).

3. There are the 3 constraints coming from requiring the equalities: $M_Y = M_{Y'}$, $M_X = M_{X'}$, and $M_N = M_{N'}$.

4. Thus, for each event, since $(8-2)-3=3$ we see that if we know the 3 masses, then we can solve for the 4-momenta of the N and N' and vice versa.

The equations are quartic, and so there can be 4, 2 or 0 solutions (with acceptable positive real energies for the N and N'). If not 0, then the event is "solved" for those particular mass choices.

5. For each event, we scan through the mass space to see if one or more of the discrete solutions is acceptable.

   Each event then defines a 3-dimensional region in the 3-dimensional mass space that is physically acceptable.

6. As we increase the number of events the 3-dimensional mass region consistent with all events becomes smaller.

   However, in general (and in practice) this region will not shrink to a point.

   Thus, we need additional methods to pick out the correct point in mass space.

- To illustrate our approach, we can consider the explicit example

$$\widetilde{\chi}_2^0\widetilde{\chi}_2^0 \to \ell\widetilde{\ell}\ell\widetilde{\ell} \to \ell\ell\widetilde{\chi}_1^0\ell\ell\widetilde{\chi}_1^0 \quad ,$$
$$i.e. \quad Y = Y' = \widetilde{\chi}_2^0, \quad X = X' = \widetilde{\ell}, \quad N = N' = \widetilde{\chi}_1^0 \, ,$$

which we generate as a subcomponent of

$$\widetilde{q}\widetilde{q} \to q\widetilde{\chi}_2^0 q\widetilde{\chi}_2^0 \to \ldots \to q\ell\ell\widetilde{\chi}_1^0 q\ell\ell\widetilde{\chi}_1^0 \,. \tag{11}$$

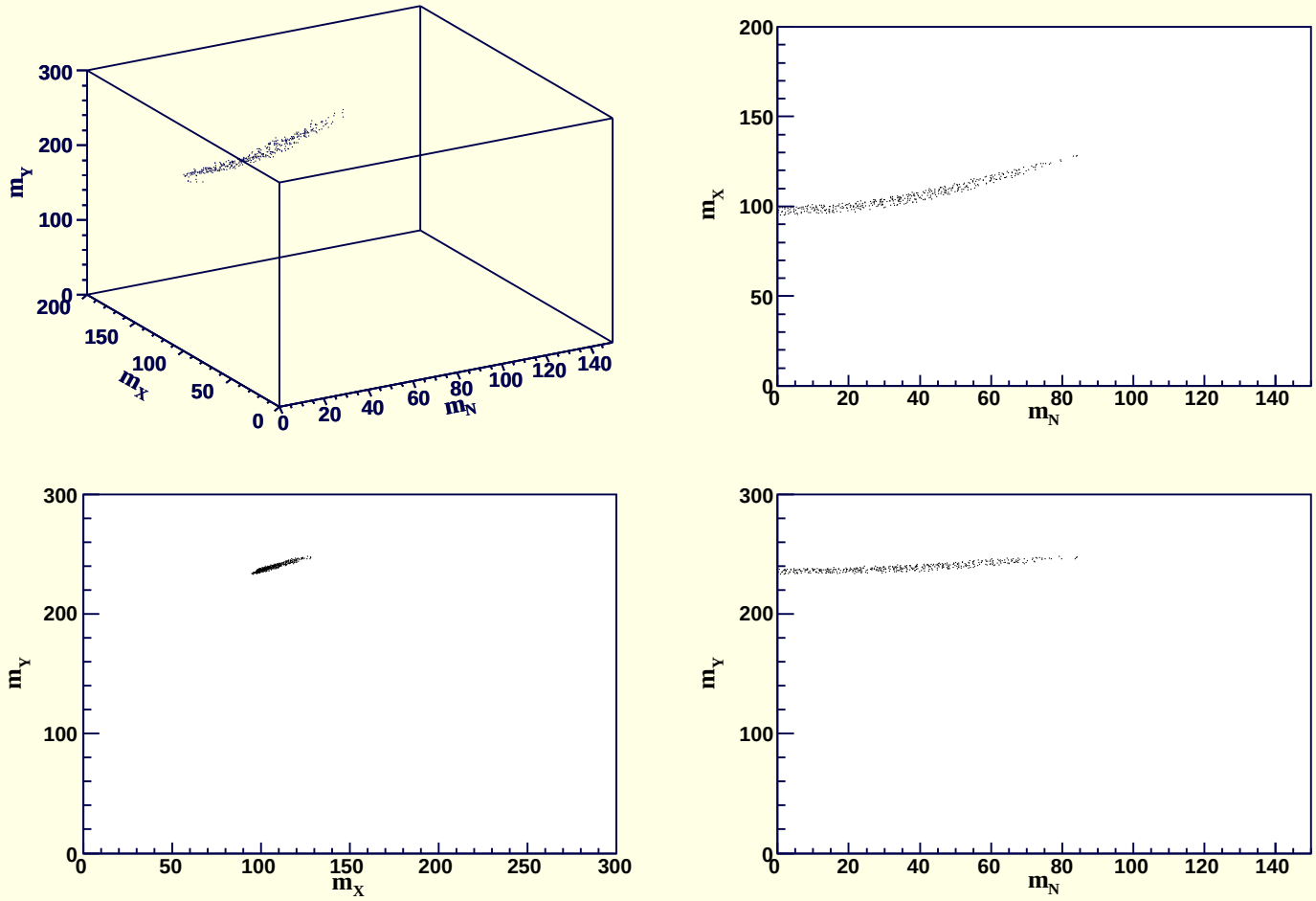

Figure 12: *Mass region (in GeV) that can solve all events.* $\mathbf{500}$ *generated events for* $m_Y = 246.6$ GeV, $m_X = 128.4$ GeV *and* $m_N = 85.3$ GeV, *using correct chain assignments and perfect resolution. Masses from 'Model I', with large* $m_{\widetilde{\chi}_2^0}$.

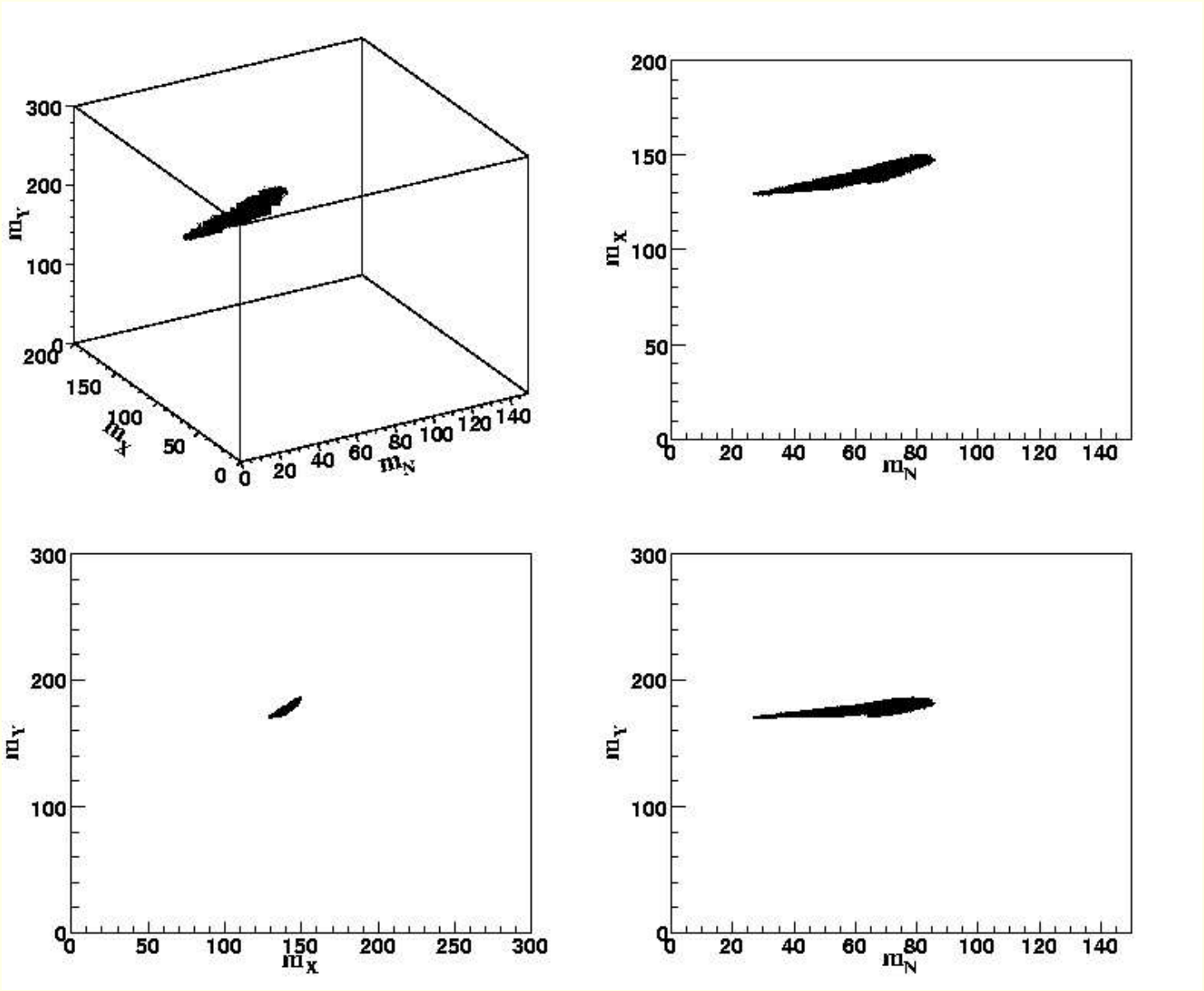

Figure 13: *Mass region (in GeV) that can solve all events.* $\mathbf{500}$ *generated events for* $m_Y = 180.8$ GeV, $m_X = 147.1$ GeV *and* $m_N = 85.2$ GeV, *using correct chain assignments and perfect resolution. The masses are from 'Model II', chosen to have masses similar to SPS1a.*

We found that the correct masses lie at the end point of the allowed region. A graphical picture is:

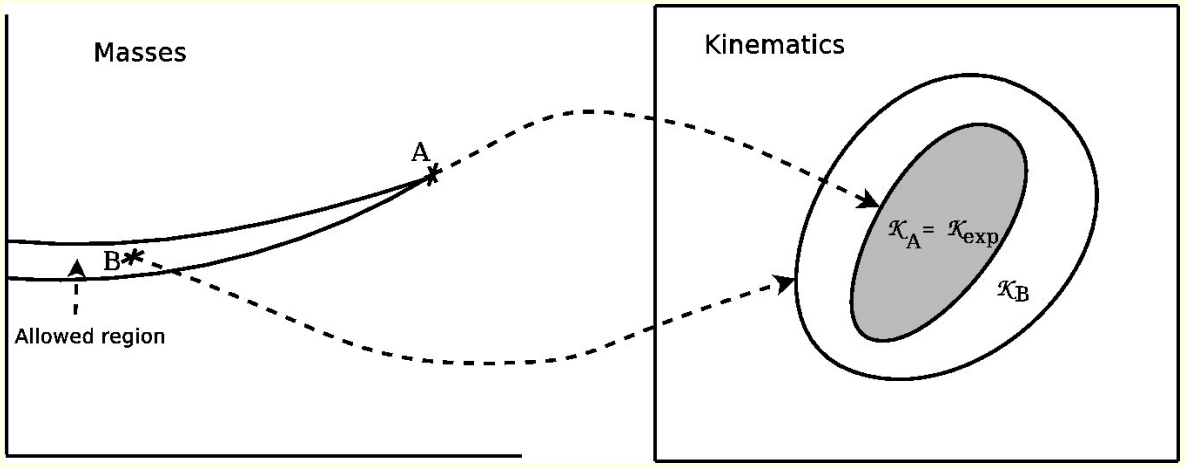

Figure 14: *Map between mass space and kinematic space. The nominal masses, point A, produces a kinematic region that coincides with the experimental region: $\mathcal{K}_A = \mathcal{K}_{exp}$. A point B inside the allowed mass region produces a larger kinematic region: $\mathcal{K}_B \supset \mathcal{K}_{exp}$.*

The kinematic space $\mathcal{K}$ refers to the set of observable momenta of the 4 leptons in the chain.

The allowed masses in $\mathcal{M}$ space are those for which every point in the $\mathcal{K}_{exp}$ part of $\mathcal{K}$ space produces at least one acceptable set of $\vec{p}_N$ and $\vec{p}_{N'}$, $i.e.$ is 'solved'.

a) The correct set of masses, $\mathcal{M}$ at point A in Fig. 14, produces a kinematic region $\mathcal{K}_A$ that coincides with the experimental one, $\mathcal{K}_A = \mathcal{K}_{exp}$, as long as the experimental statistics is large enough.

b) A different mass point produces a region that is either smaller or larger than $\mathcal{K}_{exp}$[1].

c) If smaller, the mass point does not appear in the mass region for which **all** events are solved.

d) If larger, all events are solved; we denote this kind of point, with mass set $\mathcal{M}'$, as point B in Fig. 14.

e) Let us shift the masses slightly to $\mathcal{M}' + \delta\mathcal{M}'$.

- If the kinematic region for which we have acceptable solutions still covers $\mathcal{K}_{exp}$, then $\mathcal{M}' + \delta\mathcal{M}'$ is still within the allowed region.
- Apparently, point B, which produces a region larger than K_{exp}, has the freedom to move in all directions and must live inside the allowed region.
- On the other hand, the correct mass point A, which produces exactly $\mathcal{K}_{exp}$, has the least freedom to move and must be located at an end point of the allowed region.

However, with finite resolutions and combinatorics (which lepton goes where

[1] In general cases, there could exist degenerate points that produce exactly the same kinematic region as the correct one. It is impossible to raise the degeneracy using pure kinematics.

in the two chains), not all events can be solved by the correct mass point.

$\Rightarrow$ The correct mass point will not lie within the intersection region (assuming there is any such region left).

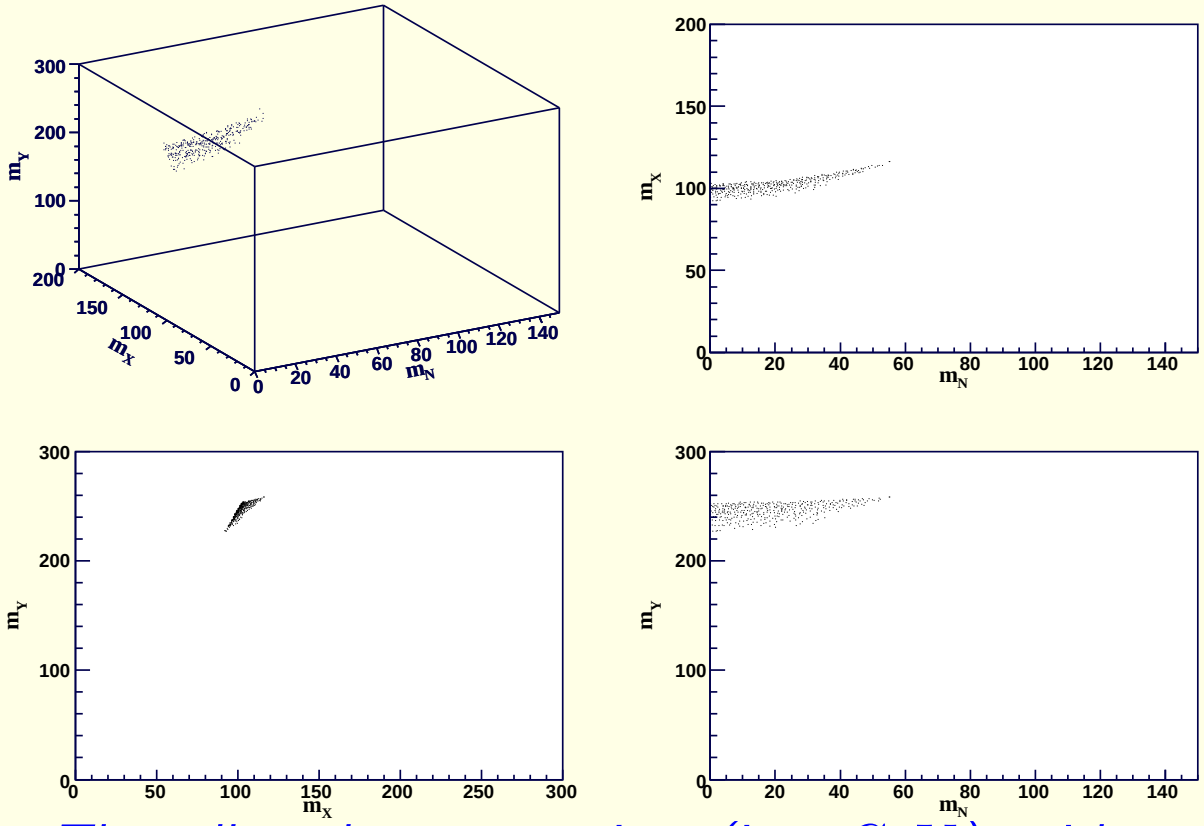

Figure 15: *The allowed mass region (in* GeV*) with smearing (ALTFAST) and wrong combinatorics.* $\mathbf{500}$ *generated events for Model I masses:* $m_Y = 246.6\ \mathrm{GeV}, m_X = 128.4\ \mathrm{GeV}$ *and* $m_N = 85.3\ \mathrm{GeV}$*. Cuts:* $|\eta| < 2.5$*,* $p_T(\ell) > 6\ \mathrm{GeV}$*.*

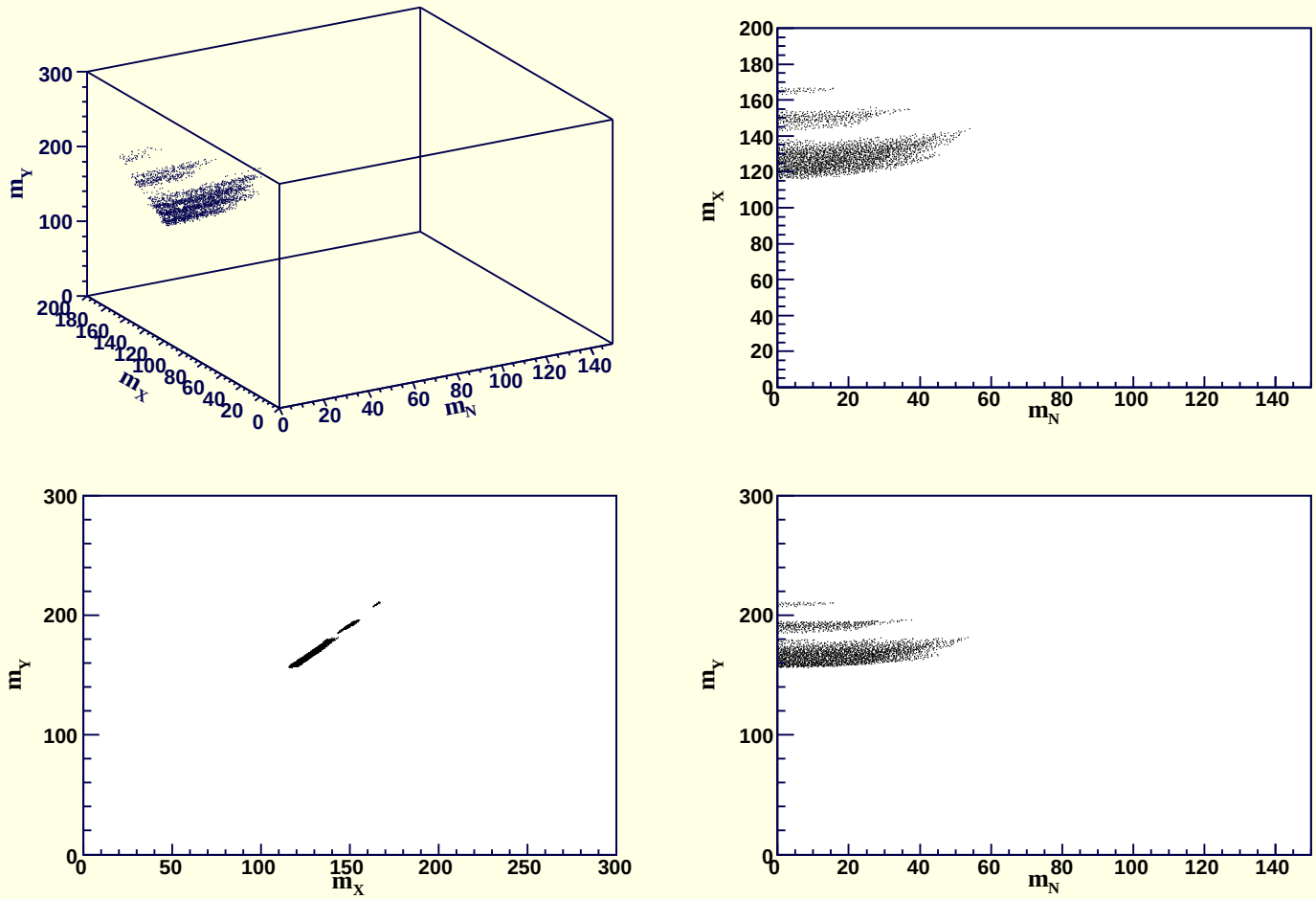

Figure 16: *Mass region (in* GeV*) that can solve all events.* $\mathbf{500}$ *generated events for Model II masses:* $\boldsymbol{m_Y = 180.8}$ GeV, $\boldsymbol{m_X = 147.1}$ GeV *and* $\boldsymbol{m_N = 85.2}$ GeV, *after smearing, combinatorics and cuts.*

- In the more realistic case, the correct mass choices do not correspond to an endpoint but rather correspond to the choices such that changes in the masses result in the most rapid decline in the number of solved/consistent events.

- Looking for this point of steepest decline in a 3-dimensional space is numerically difficult.

- If we fix two of the masses, and vary the $3rd$ mass, then we can usually identify the point at which the number of solved events starts a steep decline as this $3rd$ mass is changed.

  This will allow an iterative approach.

- The approach that works is to cycle through the $3rd$-mass choices, m_N, m_X and m_Y in that order, and at each stage look for the peak in the number of solved/consistent events as a function of the m_N mass each time it is the $3rd$-mass. Then, update this $3rd$-mass to the peak location.

  The 'peaks' are actually obtained by the intersection of the two fitted straight lines illustrated in the following figure, where two masses are set to their correct values and the $3rd$-mass is varied.

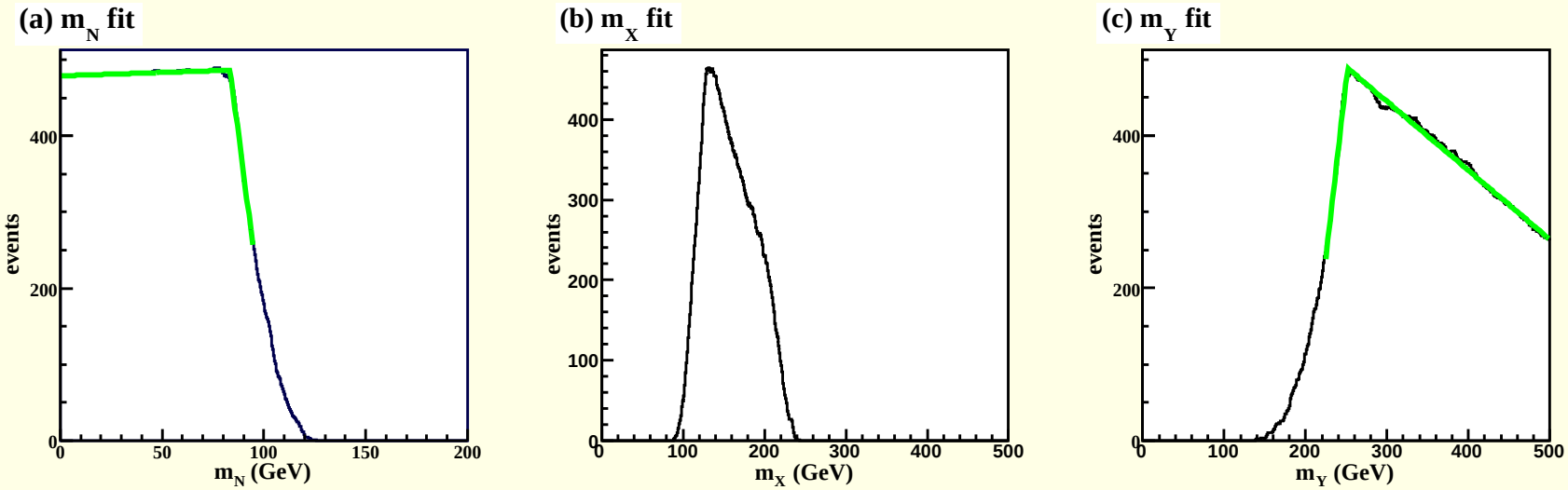

Figure 17: *One-dimensional fits by fixing the other two masses at the correct values. 500 events, combinatorics, smearing and simple cuts included. Peaks are close to correct masses.*

- **We now get more realistic. For certain soft-SUSY parameters one obtains our Model I with**

$$m_{\widetilde{g}} \sim 524, \quad m_{\widetilde{d}_L,\widetilde{s}_L} \sim 438, \quad m_{\widetilde{u}_L,\widetilde{c}_L} \sim 431$$
$$m_{\widetilde{\chi}_2^0} \sim 246.6, \quad m_{\widetilde{\mu}_R} \sim 128.4, \quad m_{\widetilde{\chi}_1^0} \sim 85.3 \qquad (12)$$

For this point, the net cross section available is

$$\sigma\left(pp \to \sum_{q,q'=u,d,c,s} \widetilde{q}_L\,\widetilde{q}'_L + \sum_{q,q'=u,d,c,s} \widetilde{q}_L\,\overline{\widetilde{q}'_L} + \sum_{q,q'=u,d,c,s} \overline{\widetilde{q}_L}\,\overline{\widetilde{q}'_L}\right) \sim 2.9 \times 10^4 \text{ fb}\,, \tag{13}$$

coming from all sources including gg fusion, $u_L u_L$ fusion, *etc.* The branching ratios relevant to the particular decay chain we examine are

$$\begin{aligned} B(\widetilde{q}_L \to q\widetilde{\chi}_2^0) &\sim 0.27 \quad (q = u, d, c, s) \\ B(\widetilde{\chi}_2^0 \to \widetilde{\mu}_R^{\pm}\mu^{\mp}) &\sim 0.124 \\ B(\widetilde{\mu}_R^{\pm} \to \mu^{\pm}\widetilde{\chi}_1^0) &= 1\,. \end{aligned} \tag{14}$$

The net effective branching ratio for the double decay chain is

$$B(\widetilde{q}_L\widetilde{q}_L \to 4\mu\widetilde{\chi}_1^0\widetilde{\chi}_1^0) \sim (0.27)^2 \times (0.124)^2 \sim 1.12 \times 10^{-3} \tag{15}$$

for any one $\widetilde{q}_L$ choice. The effective cross section for the $4\mu\widetilde{\chi}_1^0\widetilde{\chi}_1^0$ final state is then

$$\sigma(4\mu\widetilde{\chi}_1^0\widetilde{\chi}_1^0) \sim 2.9 \times 10^4 \text{ fb} \times 1.12 \times 10^{-3} \sim 32.5 \text{ fb}\,. \tag{16}$$

For an integrated luminosity of $L = 90$ fb^{-1}, this gives us 2900 $4\mu\widetilde{\chi}_1^0\widetilde{\chi}_1^0$ events before any cuts are applied.

Initial and final state radiation, resonance widths, combinatorics and experimental resolutions (as in ATLFAST) are all included.

To reduce the SM background, we require that all muons are isolated and pass the kinematic cuts:

$$|\eta|_\mu < 2.5, \quad P_{T\mu} > 10 \text{ GeV}, \quad \not{p}_T > 50 \text{ GeV}. \tag{17}$$

With these cuts, the four-muon SM background is negligible.

The number of signal events is reduced from 2900 to about 1900.

The procedure comprises the following steps:

1. Randomly select masses $m_Y > m_X > m_N$ that are below the correct masses (for example, the current experimental limits).
2. Plot the number of solved events, N_{evt}, as a function of one of the 3 masses in the recursive order m_N, m_X, m_Y with the other two masses fixed. In the case of m_Y and m_N, we fit N_{evt} for the plot with two straight lines and adopt the mass value at the intersection point as the updated mass. In the case of m_X, the updated mass is taken to be the mass at the peak of the N_{evt} plot.

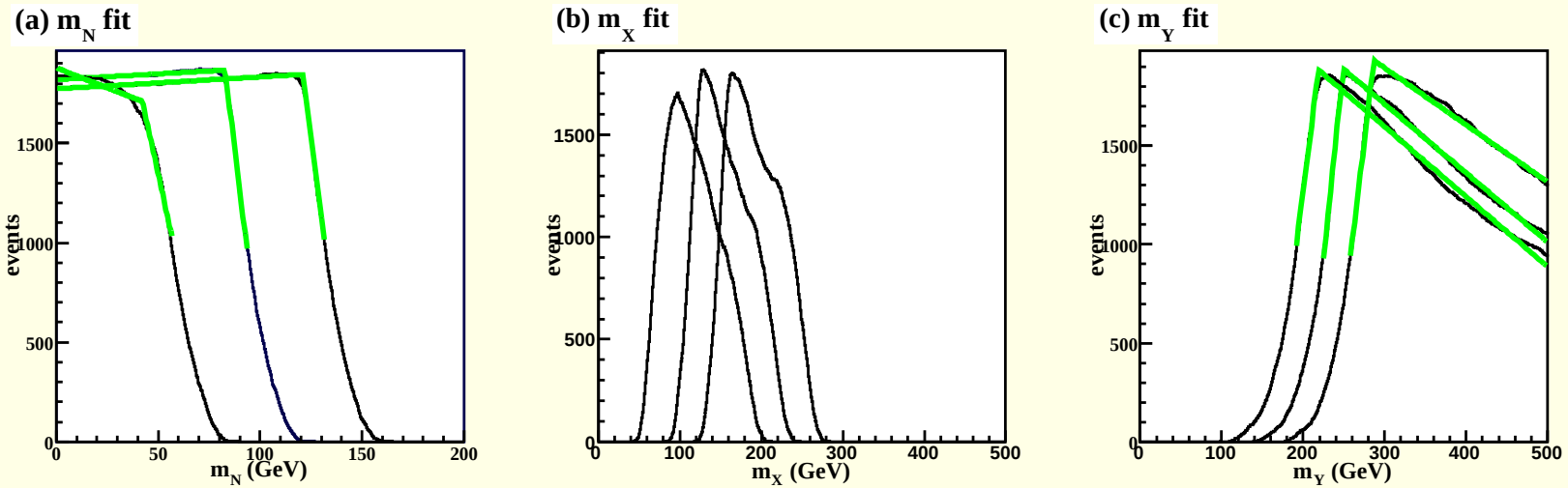

Figure 18: *A few steps showing the migration of the one dimensional fits. The middle curve in each plot corresponds to masses close to the correct values.*

A few intermediate one-dimensional fits are shown in Fig. 18.

3. **Each time after a fit to m_N, record the number of events at the intersection (sometimes called the turning point) of the two straight lines, as exemplified in Fig. 18 a. This event number at the turning point will in general be non-integer.**
4. **Repeat steps 2 and 3. The number of events recorded in step 3 will in general increase at the beginning and then decrease after some steps, as seen in Fig. 19. Halt the recursive procedure when the number of (fitted) events has sufficiently passed the maximum position.**
5. **Fit Fig. 19 to a (quartic) polynomial and take the position where the polynomial is maximum as the estimated m_N.**
6. **Keep m_N fixed at the value in step 5 and do a few one-dimensional fits**

for m_Y and m_X until they are stabilized. Take the final values as the estimates for m_Y and m_X.

- The end result is the plot below.

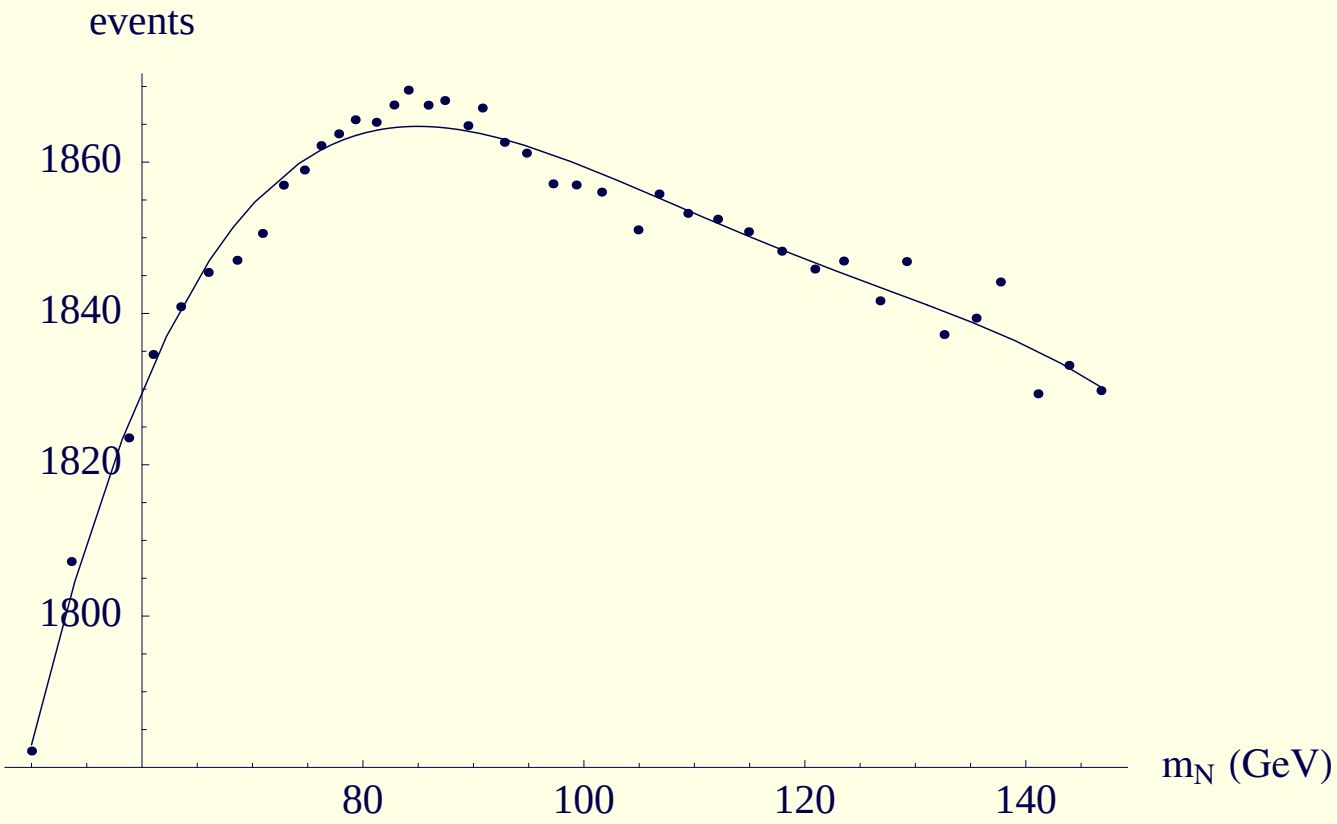

Figure 19: *The final plot for determining m_N. The position of the maximum of the fitted polynomial is taken to be the estimation of m_N..*

Remarkably, the point at which the turnover occurs gives M_N (and M_X

and M_Y) to good accuracy.

The final values for the masses in one "experiment" were determined as

$$\{252.2, 130.4, 85.0\}\ \text{GeV} \quad vs. \quad \{246.6, 128.4, 85.3\}\ \text{GeV} \tag{18}$$

Remarkably, the N mass is extremely accurate and the Y mass quite close as well.

A deeper understanding of our procedure can be gained by examining the graphical representation of the steps taken in the (m_Y, m_N) plane shown in Fig. 20.

There, we display contours of the number of (fitted) events after maximizing over possible m_X choices.

There is a 'cliff' of falloff in the number of solved events beyond about 1825 events. It is the location where this cliff is steepest that is close to the input masses, which are indicated by the (red) star.

The mass obtained by our recursive fitting procedure is indicated by the (blue) cross.

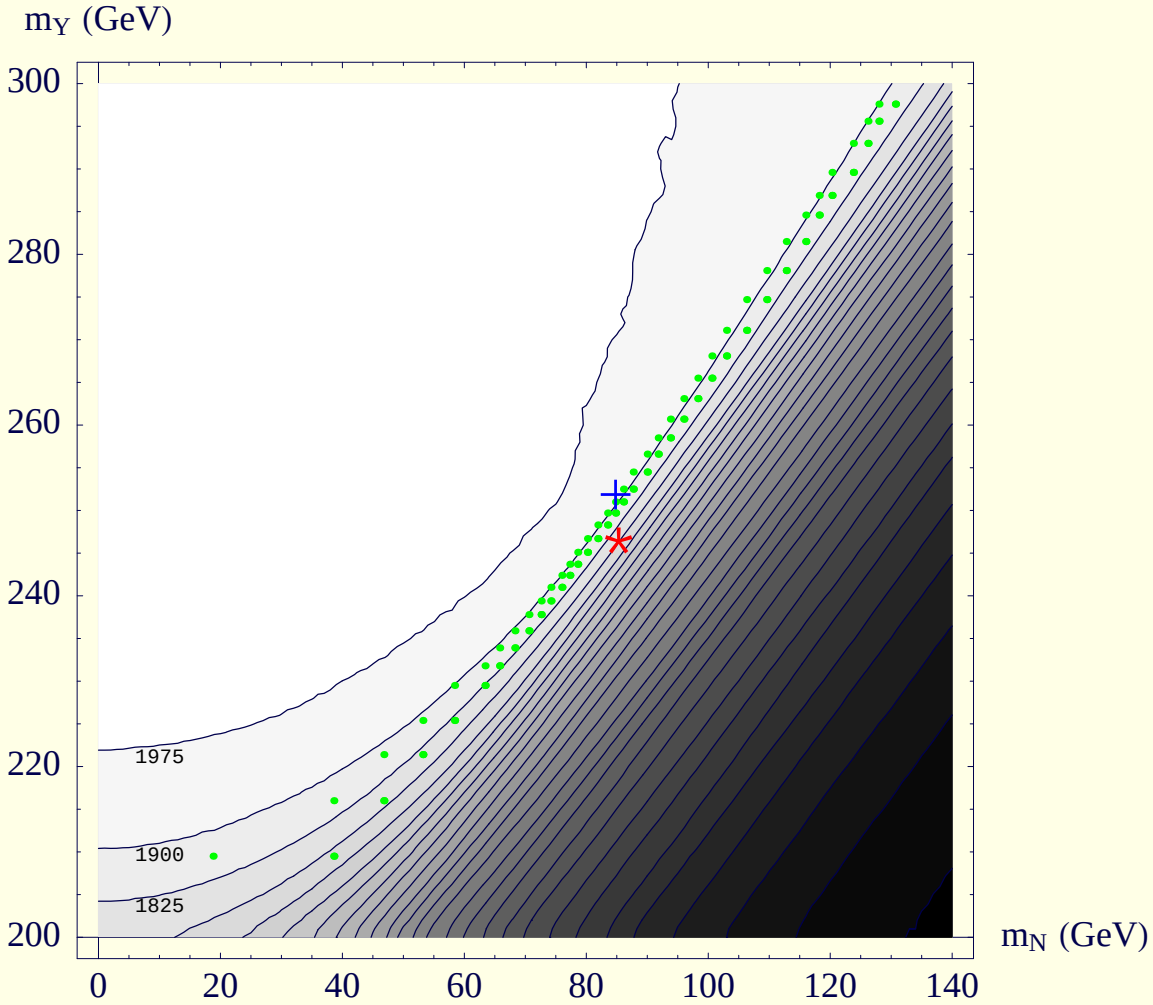

Figure 20: *Contours for the number of solved events in the $m_N \sim m_Y$ plane with 2000 events. The number of events is the maximum value obtained after varying m_X. Contours are plotted at intervals of 75 events, beginning with a maximum value of 1975. The green dots correspond to a set of one-dimensional fits. The $\star$ shows the input masses and the $+$ shows our fitted masses.*

- **Error evaluation:**

  Must adopt an 'experimental' approach for such an empirical procedure:

  Generate 10 different $90\ \mathrm{fb}^{-1}$ data samples and apply the procedure to each sample.

  Estimate the errors of our method by examining the statistical variations of the 10 samples, which yields

$$m_Y = 252.2 \pm 4.3\text{GeV}, \quad m_X = 130.4 \pm 4.3\text{GeV}, \quad m_N = 86.2 \pm 4.3\text{GeV}. \tag{19}$$

  The statistical variations for the mass differences are much smaller:

$$\Delta m_{YX} = 119.8 \pm 1.0\text{GeV}, \quad \Delta m_{XN} = 46.4 \pm 0.7\text{GeV}. \tag{20}$$

  Compared with the correct values $\mathcal{M}_A = \{246.6, 128.4, 85.3\}$, we observe small biases in the mass determination, which means that our method has some "systematic errors".

  However, these systematic errors are determined once we fix the experimental resolutions, the kinematic cuts and the fit procedure.

Therefore, they can be easily corrected for, which leaves us errors for the absolute mass scale of $\sim$ *few* GeV and for the mass differences of ~ 1 GeV.

- **Backgrounds**

In the above example, the background is negligible with the applied cuts.

However, if in some other case the backgrounds turned out to be substantial, they could decrease the accuracy of the mass determination.

Instead of analyzing another process with sizable backgrounds, we stick to the four muon events studied above but make up more "backgrounds".

In particular, we consider the 4-muon events from top pair production, but unlike above we do not require the muons to be isolated (which eliminates this background).

$\Rightarrow$ a significant number of events have 4 hard muons.

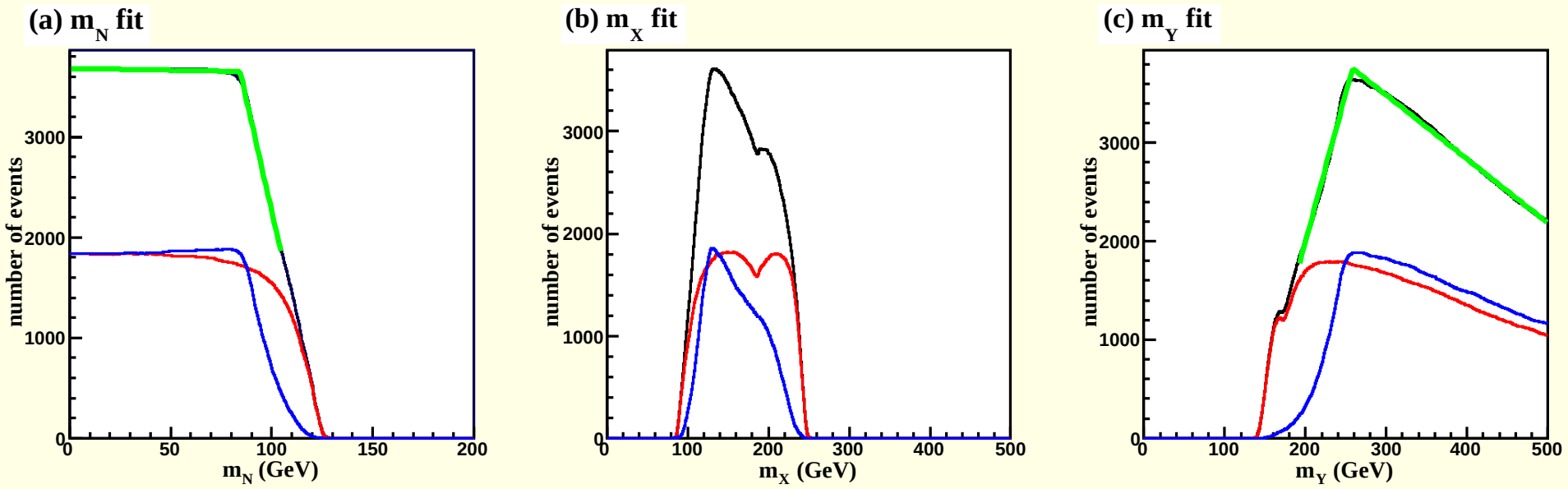

Figure 21: *Fits with $90 fb^{-1}$ signal events and an equal number of background events. Separate numbers of signal (blue) and background (red) events are also shown.*

Adding an equal number of background events to $90 fb^{-1}$ signal events, we repeat the one-dimensional fits. A typical cycle around the correct masses is shown in Fig. 21.

For comparison the number of solvable signal events and background events are also shown separately.

The effect of background events is clear: the curve for solvable background

events is much smoother around the turning point, and therefore smears but does not destroy the turning point.

Although we are considering one specific background process, this effect should be generic, unless the backgrounds happen to have non-trivial features around the turning points.

Nevertheless, due to the fact that there are 8 possible combinations, the chance that a background event gets solutions is quite large and they do affect the errors and biases of the mass determination.

This can be seen in Fig. 22, in which we have used the same 10 sets of signal events as in the previous subsection, but varied the number of background events according to the ratio $background/signal = 0, 0.1, 0.2, 0.5, 1$.

We observe increases in both the biases and variations.

But, if the backgrounds are understood (which if SM, they will be), then we can correct for them.

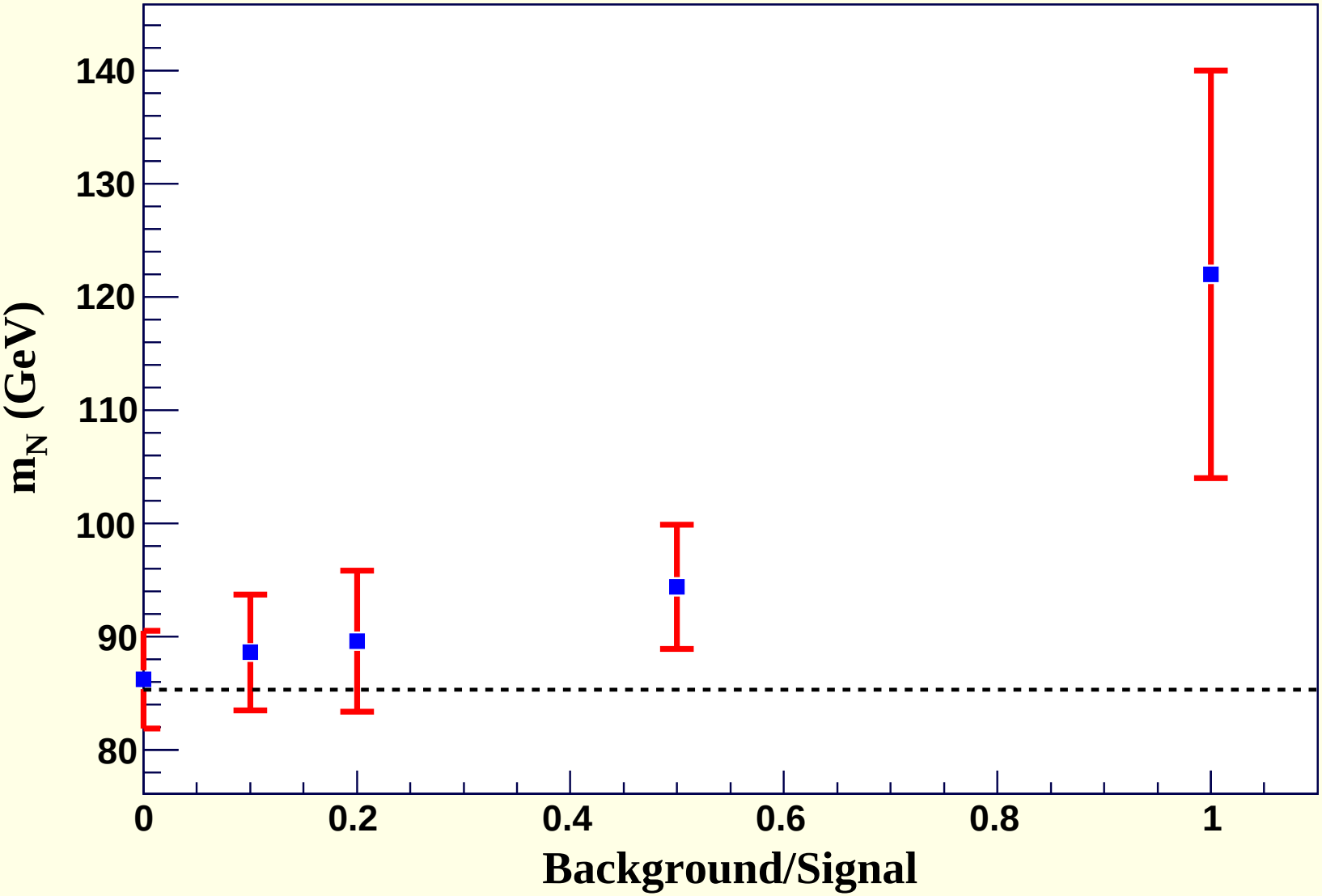

Figure 22: *m_N determination with different background-signal ratio. The dashed horizontal line corresponds to the correct m_N.*

- **If it should be that $m_N \sim 0$, then we will know it.**

  We have found that it would quickly become apparent that we were not finding a maximum in the included event number as m_N is increased.

  We would then backtrack to $m_N = 0$ and find that actually the number of included events is largest there and declines as m_N increases. A typical plot is shown in Fig. 23.

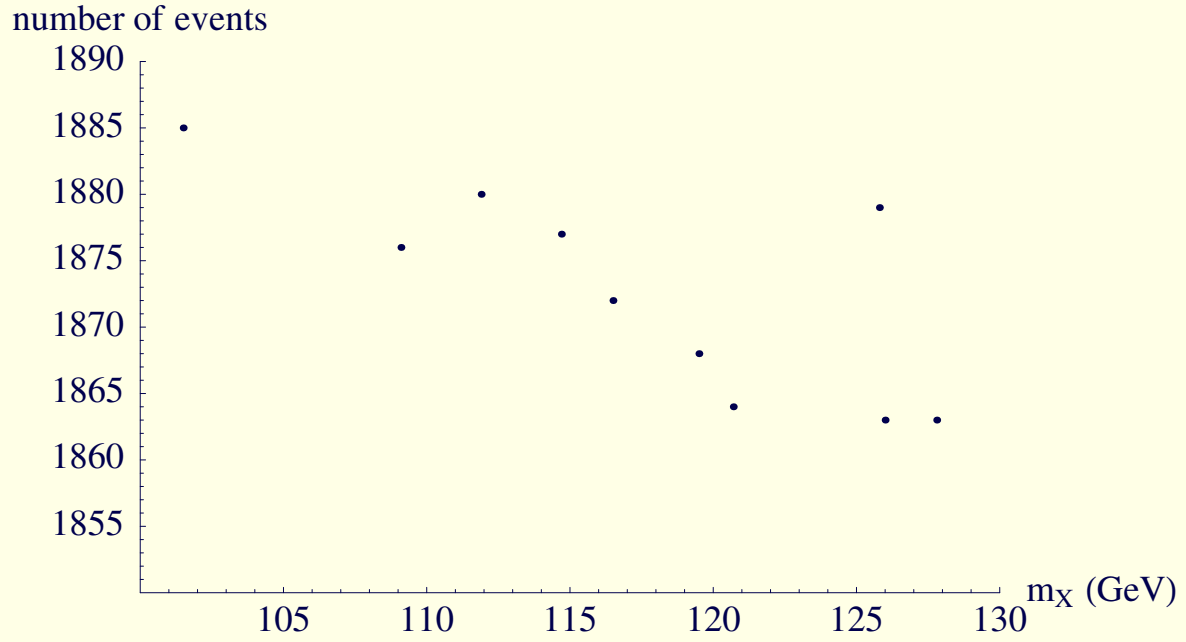

Figure 23: *m_N determination for a case with $m_Y = 199.4$ GeV, $m_X = 100$ GeV and $m_N = 0.1$ GeV. Requires very large μ in SUSY model. 2000 event sample.*

- **Peculiar mass separation choices can give some special features.**

  We are currently working on optimizing our procedures for such cases.

- **We are confident that the experimental groups will actually end up doing even better in the end.**

  In particular, if they understand the backgrounds then they can separately apply our procedure to them and subtract the background from the summed curves of Fig. 21, returning us to a situation close to the zero-background case first considered.

The SPS1a Point

- **It is desirable to compare directly to the results obtained by others for the SPS1a SUSY parameter point.**

- **We perform the analysis using the same $4\mu\widetilde{\chi}_1^0\widetilde{\chi}_1^0$ final state that we have been considering. For the usual SPS1a mSUGRA inputs the masses for $Y = \widetilde{\chi}_2^0$, $X = \widetilde{\mu}_R$ and $N = \widetilde{\chi}_1^0$ (from ISAJET 7.75) are 180.3 GeV, 142.5 GeV and 97.4 GeV, respectively.**

- This is a more difficult case than Point I considered earlier due to the fact that the dominant decay of the $\widetilde{\chi}_2^0$ is $\widetilde{\chi}_2^0 \to \tau\widetilde{\tau}_1$. The branching ratio for $\widetilde{\chi}_2^0 \to \mu\widetilde{\mu}_R$ is such as to leave only about 1200 events in the $4\mu\widetilde{\chi}_1^0\widetilde{\chi}_1^0$ final state after $L = 300\ \mathrm{fb}^{-1}$ of accumulated luminosity.

- Cuts reduce the number of events further to ~ 425.

  This is too few for our technique to be as successful as for the earlier considered cases.

- After including combinatorics and resolution we obtain:

$$m_Y = 188 \pm 12\ \mathrm{GeV}\,, \quad m_X = 151 \pm 14\ \mathrm{GeV}\,, \quad m_N = 100 \pm 13\ \mathrm{GeV}\,. \tag{21}$$

  In Fig. 24, we give an SPS1a plot analogous to Fig. 19.

  Errors are determined by generating many such plots for different samples of ~ 425 events (the exact number changes depending upon event details).

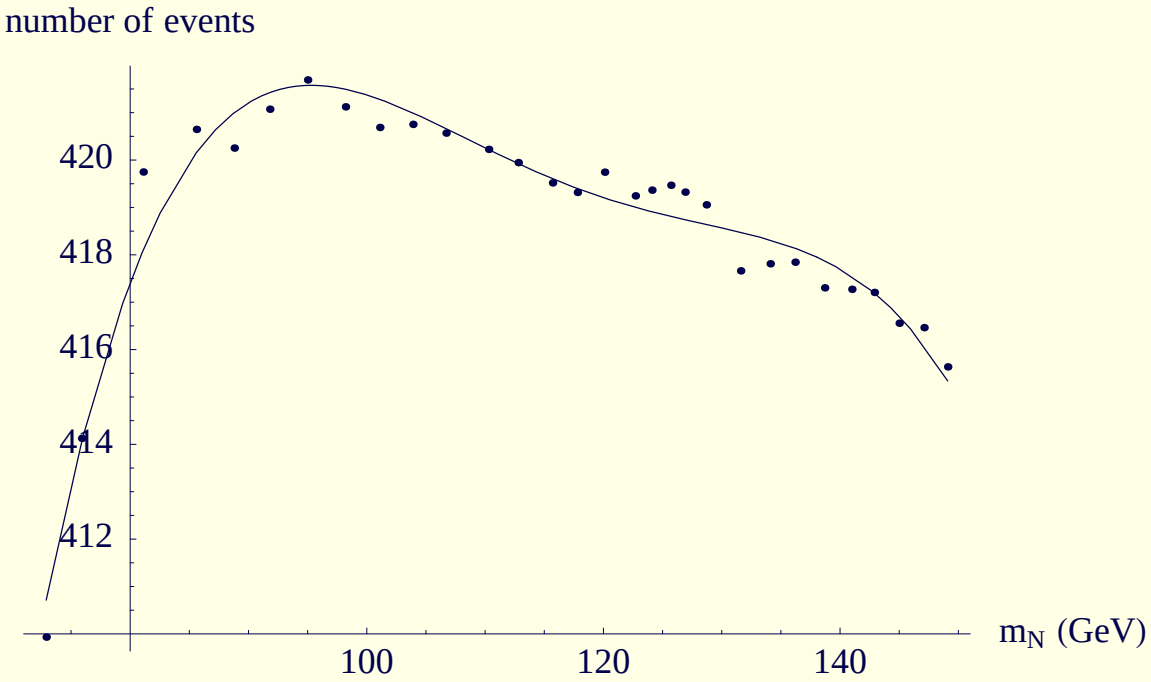

Figure 24: *Fitted number of events at the turning point as a function of* m_N *for the fits for the SPS1a case.*

Note the vertical scale. The change in the number of events as one varies m_N **is quite small for small event samples and this is what leads to the larger errors in this case.**

- **In principle, we must also take into account the fact that the** $\widetilde{\chi}_2^0 \to \tau\widetilde{\tau}_1$ **decays provide a background to the purely muonic final state.**

The dominant decay $\widetilde{\chi}_2^0 \to \tau\widetilde{\tau}_1$ has a branching ratio that is a factor of ~ 14 times larger than that for $\widetilde{\chi}_2^0 \to \ell\widetilde{\ell}_R$. [2]

The $\widetilde{\tau}_1$ will then decay to $\tau\widetilde{\chi}_1^0$.

If both τ's then decay to $\mu\nu\overline{\nu}$, then $\widetilde{\chi}_2^0 \to \tau\widetilde{\tau}_1$ events will be likely to contaminate the $\widetilde{\chi}_2^0 \to \mu\widetilde{\mu}_R$ sample.

Fortunately, this contamination is not huge. The relevant effective branching ratios for $\widetilde{\chi}_2^0\widetilde{\chi}_2^0 \to \tau\widetilde{\tau}_1\tau\widetilde{\tau}_1 \to 4\mu\widetilde{\chi}_1^0\widetilde{\chi}_1^0$ and $\widetilde{\chi}_2^0\widetilde{\chi}_2^0 \to \tau\widetilde{\tau}_1\mu\widetilde{\mu}_R \to 4\mu\widetilde{\chi}_1^0\widetilde{\chi}_1^0$ are

$$\left[\frac{B(\widetilde{\chi}_2^0 \to \tau\widetilde{\tau}_1 \to \tau\tau\widetilde{\chi}_1^0 \to \mu\mu 4\nu\widetilde{\chi}_1^0)}{B(\widetilde{\chi}_2^0 \to \mu\widetilde{\mu}_R \to \mu\mu\widetilde{\chi}_1^0)}\right]^2 \sim \left[14 \times (0.174)^2\right]^2 \sim 0.18 \quad (22)$$

and

$$2\left[\frac{B(\widetilde{\chi}_2^0 \to \tau\widetilde{\tau}_1 \to \tau\tau\widetilde{\chi}_1^0 \to \mu\mu 4\nu\widetilde{\chi}_1^0)}{B(\widetilde{\chi}_2^0 \to \mu\widetilde{\mu}_R \to \mu\mu\widetilde{\chi}_1^0)}\right] \sim 0.85\,, \quad (23)$$

respectively.

[2] This is, of course, due to the fact that $\widetilde{\chi}_2^0$ prefers to couple to left-handed slepton components, which are significant for the $\widetilde{\tau}_1$.

The contamination levels from these backgrounds are further reduced by factors of ~ 5 for the $\widetilde{\chi}_2^0\widetilde{\chi}_2^0 \to \tau\widetilde{\tau}_1\tau\widetilde{\tau}_1$ final state and by ~ 2 for the $\widetilde{\chi}_2^0\widetilde{\chi}_2^0 \to \tau\widetilde{\tau}_1\mu\widetilde{\mu}_R$ final state after imposing the simple cuts of Eq. (17) (due to the softer nature of the μ's coming from the τ decays), implying contamination at about the 3.6% and 40% levels, respectively.

Clearly, it is important to reduce this level of contamination given that $m_{\widetilde{\tau}_1}$ is smaller than $m_{\widetilde{\ell}_R}$ by about 15 GeV and so, to the extent that events containing $\widetilde{\chi}_2^0 \to \tau\widetilde{\tau}_1$ decays remain in our sample, they might contribute additional structures to our plots of number of events vs. mass.

This reduction can be accomplished on a statistical basis using a further trick analogous to that discussed (but not, we believe, actually employed) by Gjeltsen et.al.

In our case, where both chain decays are considered simultaneously, we have $4\mu\widetilde{\chi}_1^0\widetilde{\chi}_1^0$ states arising from $\widetilde{\chi}_2^0\widetilde{\chi}_2^0 \to \tau^{\pm}\widetilde{\tau}_1^{\mp}\tau^{\pm}\widetilde{\tau}_1^{\mp}$ decays and $\widetilde{\chi}_2^0\widetilde{\chi}_2^0 \to \tau^{\pm}\widetilde{\tau}_1^{\mp}\mu^{\pm}\widetilde{\mu}_R^{\mp}$ decays in addition those from our $\widetilde{\chi}_2^0\widetilde{\chi}_2^0 \to \mu^{\pm}\widetilde{\mu}_R^{\mp}\mu^{\pm}\widetilde{\mu}_R^{\mp}$ signal.

To subtract off the background SUSY events from the former two decay chains, we can employ the following subtraction (where the initial $\widetilde{\chi}_2^0\widetilde{\chi}_2^0$ and final $\widetilde{\chi}_1^0\widetilde{\chi}_1^0$ are implicit)

$$N(\mu^{\pm}\widetilde{\mu}_R^{\mp}\mu^{\pm}\widetilde{\mu}_R^{\mp} \to \mu^+\mu^-\mu^+\mu^-)$$

$$
\begin{aligned}
&= N(\mu^+\mu^-\mu^+\mu^-) - N(e^+\mu^-\mu^+\mu^-) + N(e^+e^+\mu^-\mu^-) \\
&= N(\mu^+\mu^-\mu^+\mu^-) - \tfrac{1}{4}\Big[N(e^+\mu^-\mu^+\mu^-) + N(e^-\mu^+\mu^-\mu^+) \\
&\qquad + N(\mu^+e^-e^+e^-) + N(\mu^-e^+e^-e^+)\Big] \\
&\qquad + \frac{1}{2}\left[N(e^+e^+\mu^-\mu^-) + N(e^-e^-\mu^+\mu^+)\right] .
\end{aligned}
\tag{24}
$$

and so forth, where the first form is likely to have smaller statistical error, but other forms would give guidance on statistical sensitivity.

We have not actually performed this kind of analysis using any of the possible subtractions to see how well we do, but we expect that the net background contamination will be equivalent to $B/S \lesssim 0.1$, a level for which our techniques work very well and the errors quoted earlier for the SPS1a point will not be increased by very much.

2 chains: 3 visible particles per chain

- Recall from the counting section that to solve requires just $n = 2$ events.

  There are many ways to set up the equations. The most convenient form leads (for 2 events) to 3 simultaneous quadratic equations.

  There are multiple solutions to these equations for any 2 events, even before including combinatorics and resolution.

  However, before combinatorics and resolutions, typically only one of the multiple solutions is common to all pairs of events that one can consider.

  It is easy to get lots of pairs of events; for example, 58 events leads to 1653 pairs.

  We again focus on the decay chain $\tilde{q} \to q\tilde{\chi}_2^0 \to q\mu\tilde{\mu}_R \to \tilde{\chi}_1^0 q\mu\mu$ with SPS1a masses $m_{\tilde{q}} = 565$ GeV, $m_{\tilde{\chi}_2^0} = 180$ GeV, $m_{\tilde{\mu}_R} = 142$ GeV and $m_{\tilde{\chi}_1^0} = 97$ GeV.

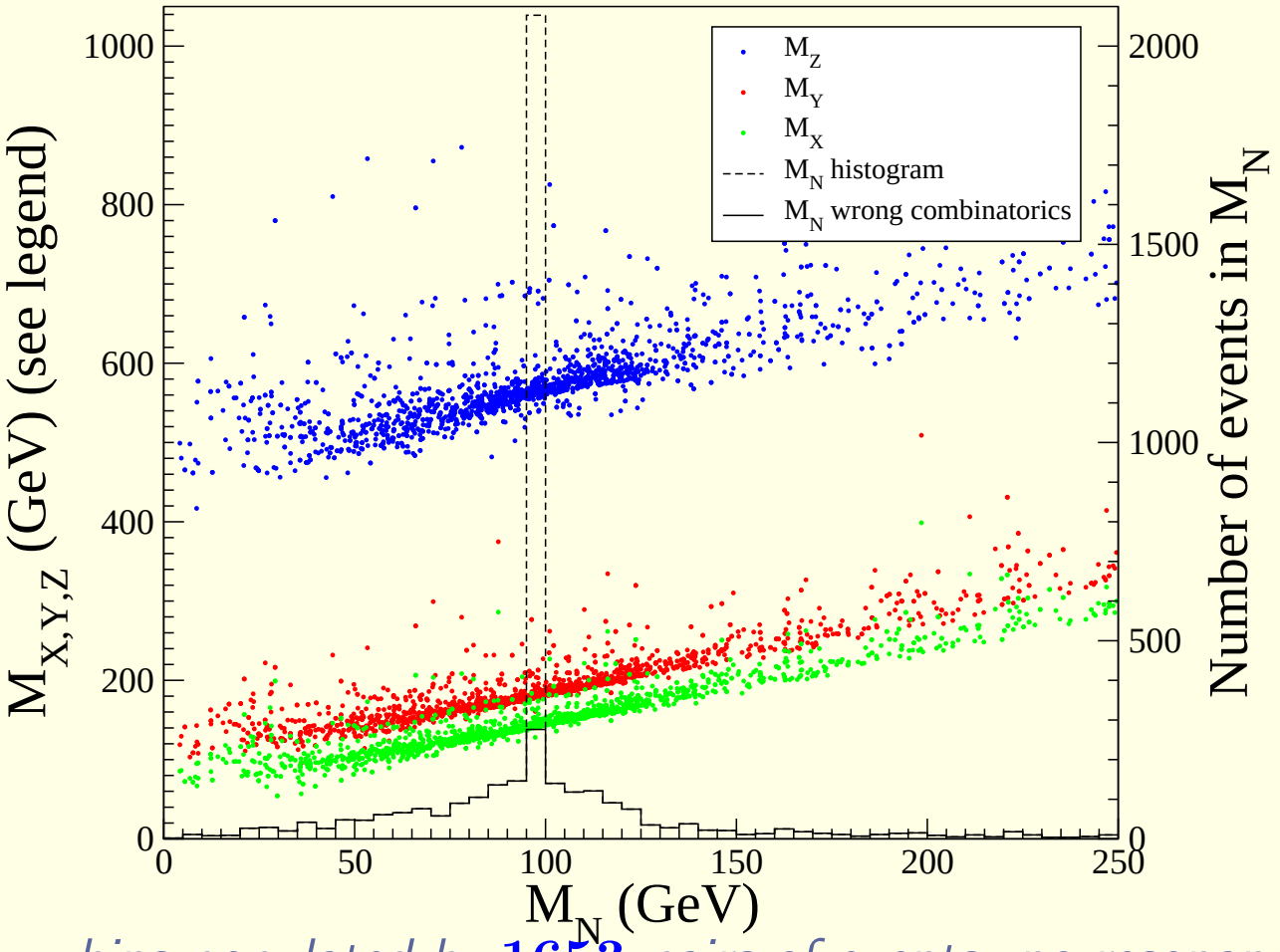

Figure 25: *m_N bins populated by* **1653** *pairs of events: no resonance width effects are included, all squarks are taken degenerate and no resolution effects are included, but correct combinatoric uncertainties are and give the "pedestal".*

In the above plot, you see the ideal situation: narrow width approximation for all the intermediate states; exactly degenerate squark masses (vs. the real SPS1a masses that have some differences between 1st two generations); and no resolution smearing —only combinatoric reassignments are incorporated.

To be more realistic, one should do the following;

1. **generate $\widetilde{q}_L\widetilde{q}_L$ production with ISR and FSR jets turned on;**
2. **allow for squark mass differences — e.g. for SPS1a point, we find**

$$m_{\widetilde{u}_L} = m_{\widetilde{c}_L} = 565 \text{ GeV} \quad \text{vs.} \quad m_{\widetilde{d}_L} = m_{\widetilde{s}_L} = 571 \text{ GeV}\,. \tag{25}$$

3. **include the decay widths of the $\widetilde{q}_L$'s, $\widetilde{\chi}_2^0$'s, . . .**
4. **allow for combinatoric interchanges in which muons are placed in all physically possible places along the two decay chains;**
5. **allow for interchanging the two jets that we choose to associate with the primary $\widetilde{q}_L$ decays;**
   (We choose these two jets by taking those with the largest p_T's — sometimes this is not the correct choice.)
6. **smear the momenta of the jets and muons using the resolutions of ATLFAST.**

Note: When solving for consistent masses for all the particles at once, jet energy smearing, combinatorics and so forth will influence the masses extracted further down the chain for $\widetilde{\chi}_2^0, \ldots$.

$\Rightarrow$ the excellent μ momentum resolution will not help all that much.

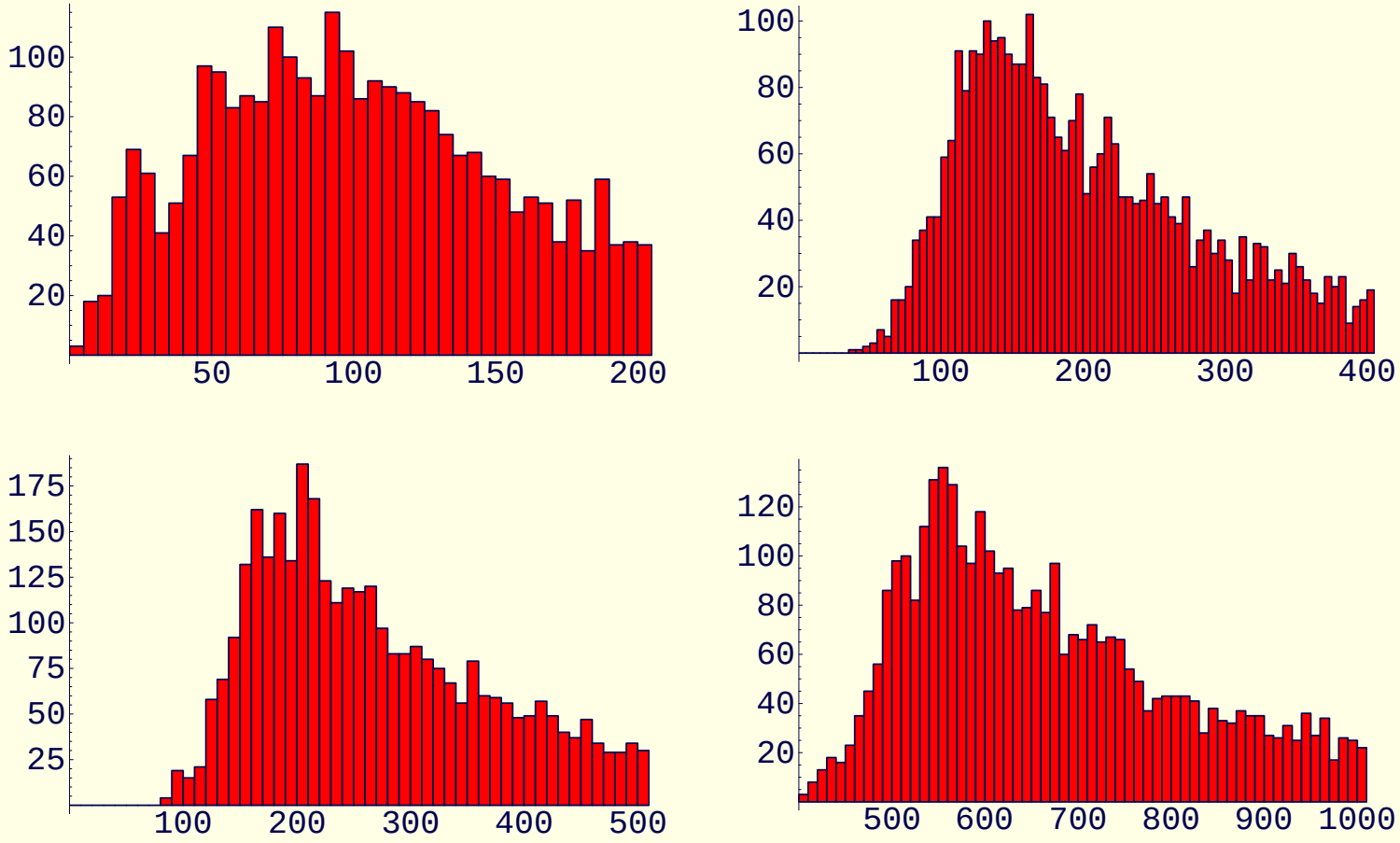

Figure 26: *Mass bins populated by* **120** *pairs of events:* *resolution effects are included,* *combinatoric interchanges are included, and* *squark mass differences and resonance widths are included.*

Target SPS1a masses: $m_{\tilde{\chi}_1^0}, m_{\tilde{\mu}_R}, m_{\tilde{\chi}_2^0}, m_{\tilde{q}} = 97, 142, 180, 565$ GeV.

Peaks are close to the actual masses.

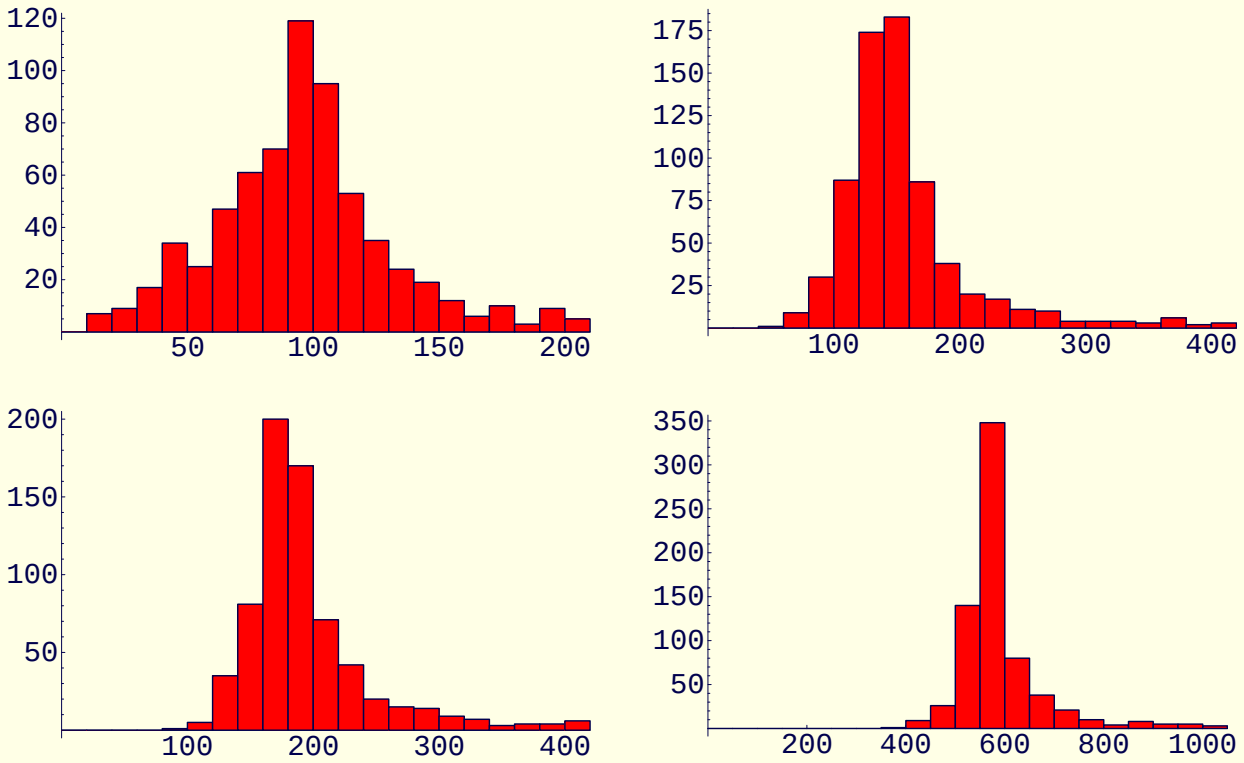

Figure 27: *Mass bins populated by* $\mathbf{500}$ *pairs of events: no resolution effects are included and correct assignments for lepton and jet positions are employed, but squark mass differences and resonance widths are included.*

Target SPS1a masses: $m_{\widetilde{\chi}_1^0}, m_{\widetilde{\mu}_R}, m_{\widetilde{\chi}_2^0}, m_{\widetilde{q}} = \mathbf{97, 142, 180, 565}$ GeV.

Squark mass differences and resonance widths, even with neither combinatorics nor resolution effects included, give substantial spread out.

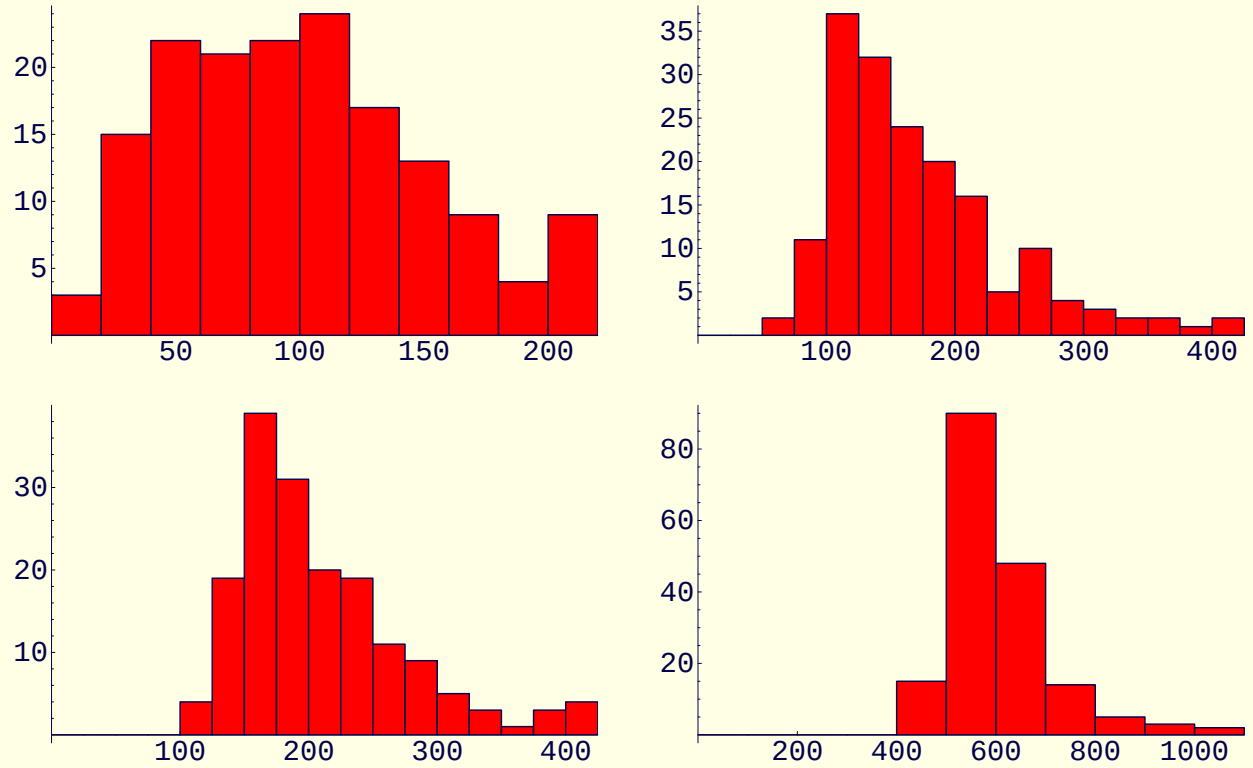

Figure 28: *Mass bins populated by* $\mathbf{500}$ *pairs of events: correct assignments for lepton and jet positions are employed, squark mass differences and resonance widths are included and resolution smearing is included.*

Target SPS1a masses: $m_{\widetilde{\chi}_1^0}, m_{\widetilde{\mu}_R}, m_{\widetilde{\chi}_2^0}, m_{\widetilde{q}} = \mathbf{97, 142, 180, 565}\ \mathrm{GeV}$.

Putting in resolution smearing (as well as squark mass difference and resonance widths) but not combinatoric rearrangements is enough to broaden and shift peaks substantially.

- **We found the following trick to help greatly.**

  In the above, there was no constraint that when you extracted the Z, Y, X, N masses from one pair of combinatoric choices for each event in one pair of events that the masses should ALL be close to the Z, Y, X, N masses, respectively, as extracted using a given pair of combinatoric choices for each of another pair of events. Most often, there is at least one bad mismatch.

  Label the masses from pair 1 for some combinatoric setup with superscript 1 and those from pair 2 for some combinatoric arrangement with superscript 2.

  Cycle through all combinatoric choices for all 4 events being considered in the case of a given pair of 2-event pairs.

  Pick out only those choices (if any) for which Δm is below some cutoff, where

$$\Delta m^2 = (m_Z^1 - m_Z^2)^2 + (m_Y^1 - m_Y^2)^2 + (m_X^1 - m_X^2)^2 + (m_N^1 - m_N^2)^2 \quad (26)$$

  Many bad combinatoric choices, badly resolution distorted cases, and far off-shell resonance cases are discarded in this way. If the cutoff is low, many 2-event pairs will not give any satisfactory case.

For any setup that gives small enough Δm plot the average mass, $\overline{m}_I \equiv \frac{1}{2}(m_I^1 + m_I^2)$, where $I = Z$, Y, X, or N.

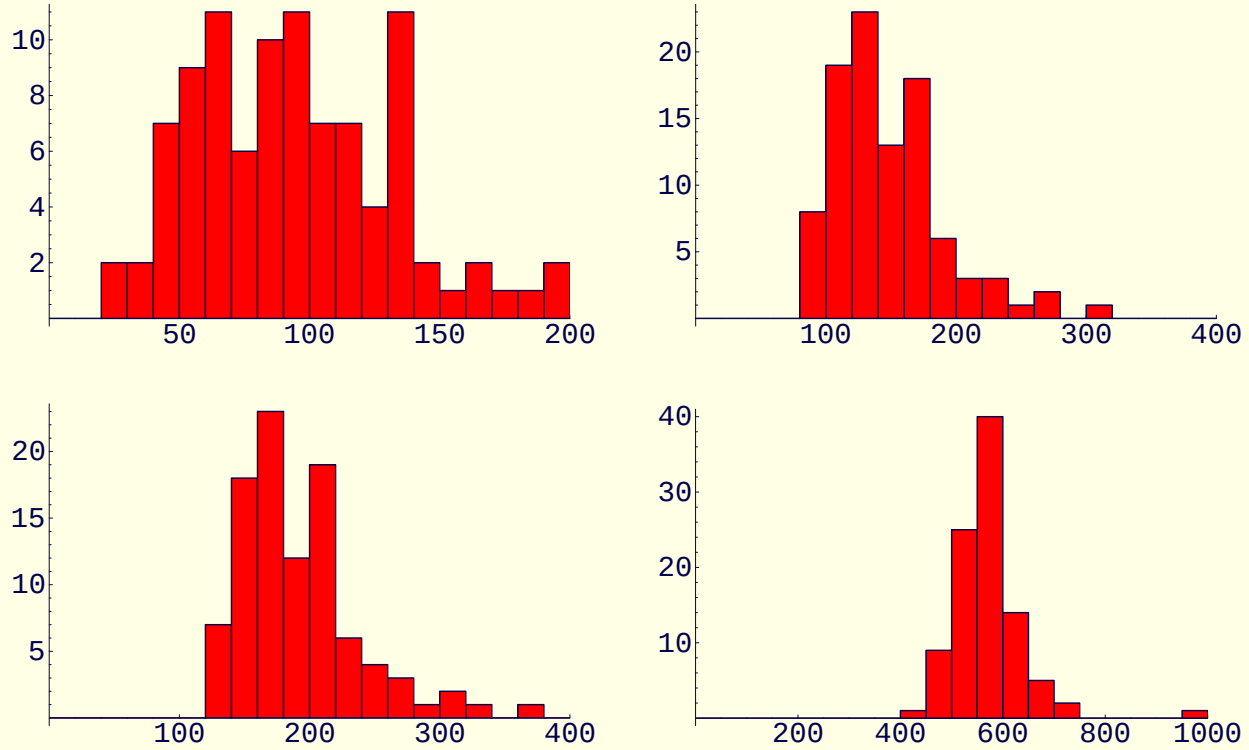

Figure 29: *Mass bins populated by considering all* $\mathbf{120 \times 119/2}$ *sets of* $\mathbf{2}$*-event pairings from* $\mathbf{120}$ $\mathbf{2}$*-event pairs: resonance width, squark mass difference, combinatorics and resolution smearing are all included. For this figure, we take* $\mathbf{\Delta m = 40}$ GeV *as the cut on the root mean square of the "distance" between masses for the two* $\mathbf{2}$*-event pairs.*

Target SPS1a masses: $m_{\tilde{\chi}_1^0}, m_{\tilde{\mu}_R}, m_{\tilde{\chi}_2^0}, m_{\tilde{q}} = 97, 142, 180, 565$ GeV.

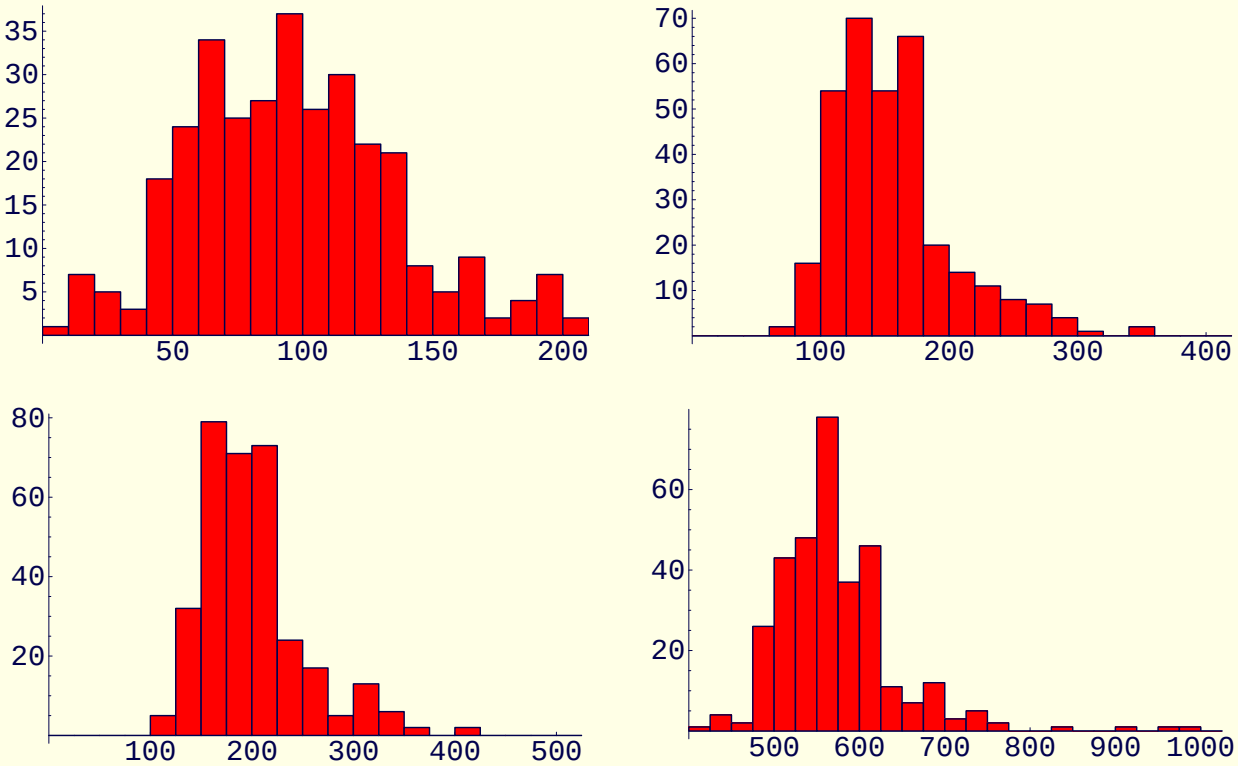

Figure 30: *As in Fig. 29 but for* $\boldsymbol{\Delta m = 90}$ GeV.

Target SPS1a masses: $\boldsymbol{m_{\tilde{\chi}_1^0}, m_{\tilde{\mu}_R}, m_{\tilde{\chi}_2^0}, m_{\tilde{q}} = 97, 142, 180, 565}$ GeV.

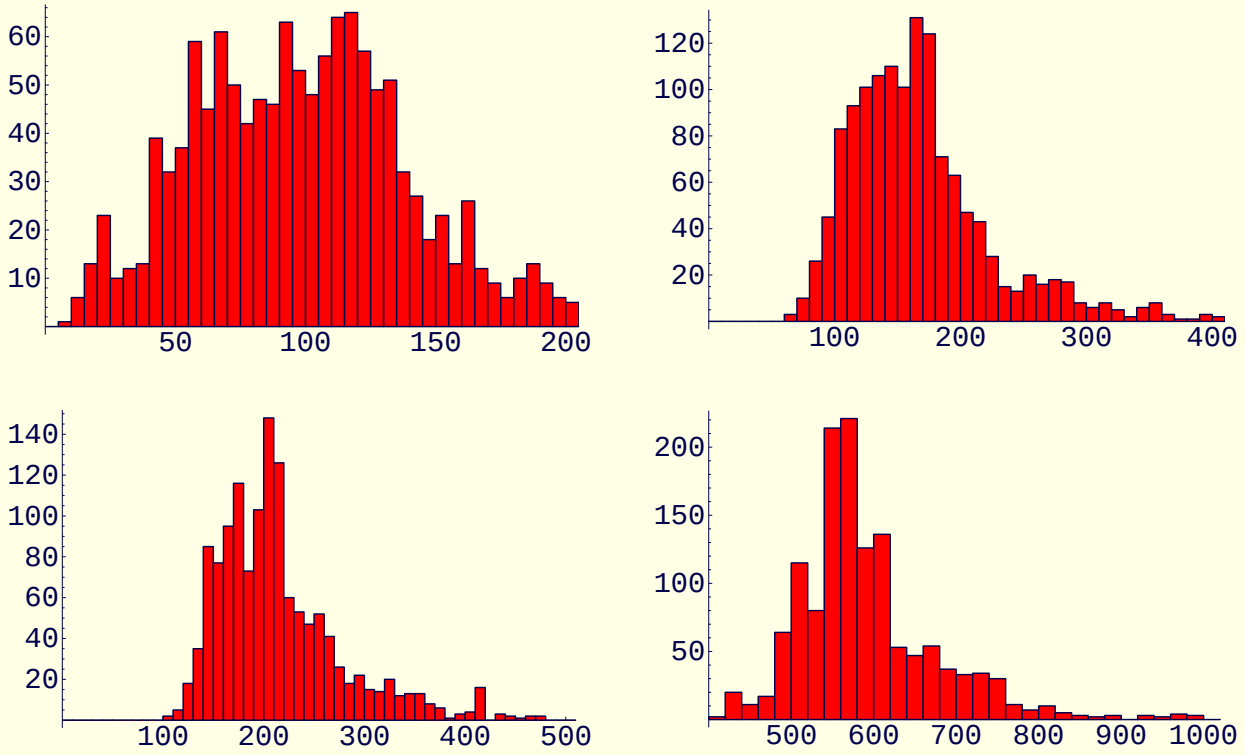

Figure 31: *As in Fig. 29 but for* $\Delta m = 400$ GeV.

Target SPS1a masses: $m_{\widetilde{\chi}_1^0}, m_{\widetilde{\mu}_R}, m_{\widetilde{\chi}_2^0}, m_{\widetilde{q}} = 97, 142, 180, 565$ GeV.

For getting a given mass m_I right, there is a best choice for Δm, but the best choice is not always the same for different I. With further study, we might be able to establish some "rules".

Bottom line: it is not clear yet that the 3-visible per chain analysis will improve over the 2-visible per chain mass determinations for the $\widetilde{\chi}_2^0$, $\widetilde{\mu}_R$ and $\widetilde{\chi}_1^0$. Of course, it is required for determining the (average) $\widetilde{q}$ mass.

Conclusions

- **Using 4 visible particles, $\sim$ *few* GeV to 10 GeV accuracy for the absolute mass scale is achievable at the LHC, depending upon the number of events available.**

- **Using more visible particles is likely to improve further on this result — but further work is required to prove this.**

  What we are in the process of doing is to fit the peaks (as we did in the previous case) and then run many experiments to see what the actual errors are on the peak location — the widths of the distributions do not necessarily reflect the mass uncertainties.

  Consequences:

  1. **This should be sufficient to eliminate the 'slider' degeneracies of the LHC inverse solutions.**
  2. **Such accuracy for the more massive states will aid enormously in the GUT extrapolation.**
  3. **It will greatly increase the accuracy of the dark matter calculation.**

- **The ability to get an absolute mass scale out of LHC data could be quite crucial for determining whether the ILC500 is sufficient or one needs to go to ILC1000.**

- **Our technique can, of course, be combined with the other techniques outlined at the beginning to obtain the best possible overall mass scale and mass differences.**

- **Don't forget that we must understand how to single out a single topology ($i.e.$ suppress others adequately) in the case that there are many new physics topologies.**

  If this cannot be done, then we must learn how to work with multiple topologies. We believe our techniques can be generalized to such a situation.